Chemical and multi-physical characterization of agro-resources' by-product as a possible raw building material

Marie Viel, Florence Collet, Christophe Lanos

Chemical and multi-physical characterization of agro-resources' by-product as a possible raw building material

Marie Viel*, Florence Collet and Christophe Lanos
* Corresponding author: marie.viel@univ-rennes1.fr
Université de Rennes, Laboratoire Génie Civil et Génie Mécanique, BP 90422, Rennes, France

Abstract

The aim of this paper is to find out the best valuation of agro-resources' by-products as new alternative raw building materials that meet to sustainable development requirement. Five agro-resources are considered: flax, hemp, corn, rape and wheat. In the present work, the chemical characteristics of bio-aggregates are studied by FTIR, Van soest method and Phenol sulfuric method to identify their composition. The investigated physical properties are particle size distribution, density, porosity, water absorption, thermal conductivity and moisture buffer value. The studied materials differ on a chemical and a thermal point of view while they all are excellent hygric regulators. These results suggest that agro-resources can be used as a raw building materials for several types of use: as lightweight aggregates or as binder.

Keywords

Sustainable building materials ; Hemp shiv; Flax shiv; Rape straw; Wheat straw; Corn cob

Abbreviations

ADF: Acid Detergent Fiber; ADL: Acid Detergent Lignin; ATR: Attenuated Total Reflectance; FTIR: Fourier Transform InfraRed spectroscopy; IRA: Initial Rate of Absorption; MBV: Moisture Buffer Value; NDF: Neutral Detergent Fiber; PSD: Particle Size Distribution; SEM: Scanning Electron Microscopy.

1. Introduction

In recent years, the quantity of agricultural waste has been rising rapidly all over the world and it will continue to increase rapidly. Taking Europe as an example, from agro-resources production in 2015 ("Agricultural production - crops," 2016), the availability of crop residues such as stems or leaves for 12 of the EU's most produced crops can be estimated. The total residue production is calculated by applying two coefficients (field residue production ratio and processing residue production ratio) on the quantity of crop production. There is as many agricultural waste as crop production. Moreover, one-third of the total residue production remains in fields and another third is used for livestock and horticulture. The last third corresponds to available crop residues (Searle and Malins, 2013). On the other hand, estimates on the availability of crop residues in 2020 in Europe, have been produced by Bloomberg New Energy Finance (Bloomberg New Energy Finance, 2010). The comparison of estimated productions with 2015 productions shows that the availability of crop residues will nearly double in 5 years' time (Table 1 and Figure 1).

Table 1: Calculation of total agricultural residue production in Europe in 2015 and projected availability of crop residues in 2020

Biomass	Crop production in 2015 (Mtonnes) ("Agricultural production - crops," 2016)	Field residue production ratio (Searle and Malins, 2013)	Processing residue production ratio (Searle and Malins, 2013)	Total residue production in 2015 (Mtonnes)	Total residue availability in 2015 (Mtonnes)	Total residue availability in 2020 (Mtonnes) (Kretschmer et al., 2012)
Wheat straw	125	0.94	0.24	148	49	74
Barley straw	49	0.94	0.24	58	19	26
Rye residues	4	1.13	0.24	9	3	6
Maize stover (corn)	54	0.80	0.47	68	23	18
Sugar beet residues	76	0.27	0.00	21	7	38
Other agricultural residues	28	1.04	0.24	34	11	56
Sum	337	-	-	338	113	218
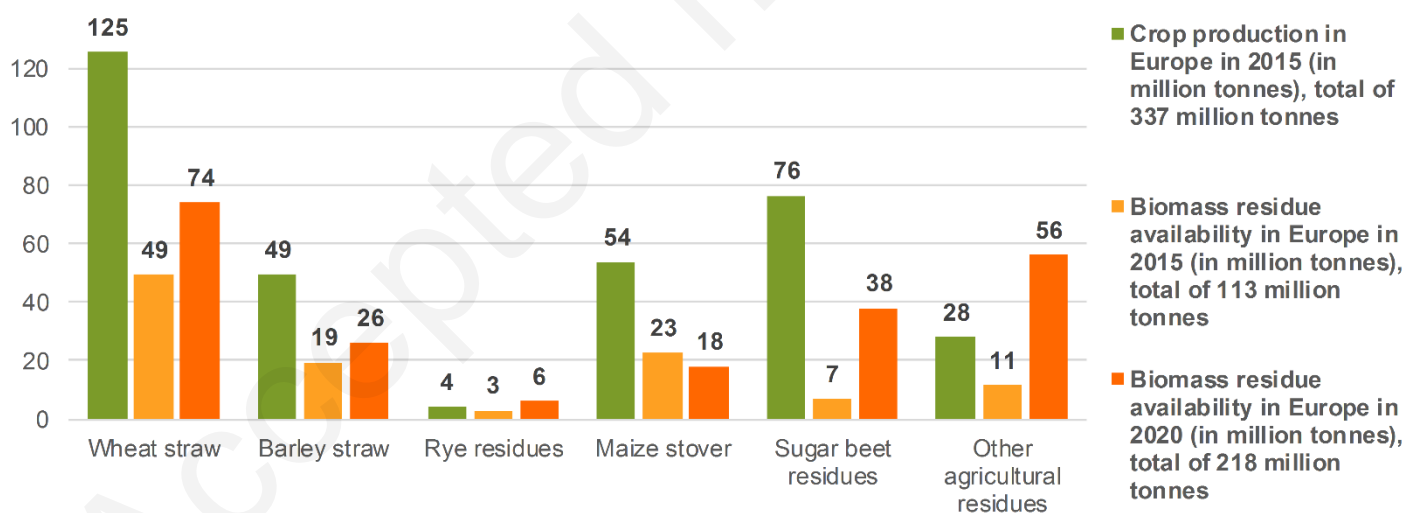
Figure 1: Crop production and biomass residue availability in Europe in 2015 compared to biomass residue availability in Europe in 2020

As a result, the environmental problems and negative impacts of agricultural waste draw more and more attention. Therefore, there is a need to adopt proper approaches to reduce and reuse agricultural waste. The agricultural residues mainly consist of different straws, such as wheat or corn. A wide range of agricultural waste could potentially be used to produce bio-based materials, aiming at the valorization of the whole biomass and basing on a zero-waste concept, such as biofuels, food and feed ingredients, chemicals and buildings materials (Fava et al., 2015; Hameed, 2014).

Recently, the Isobio project was initiated. This project, supported by the European Union Horizon 2020 program, proposes an innovative strategy to bring bio-based construction materials into the mainstream. A key innovation consists in using bio-based aggregates from a local culture with green binders to produce ecofriendly composites. This project aims to combine existing technologies in order to develop bio-based panels with low embodied energy, low carbon footprint and high hygrothermal efficiency ("ISOBIO - Naturally High Performance Insulation," 2015).

This study aims to value five agro-resources' by-products from flax, hemp, corn, rape and wheat, produced in France, to find out new alternative materials that meet the sustainable development criteria. In this work, the chemical and physical properties of these agricultural by-products, are measured and compared. Composition is studied by FTIR, Van soest method and Phenol sulfuric method to determine the content of cellulose, hemicellulose, lignin and pectin. Particles size distribution is measured by mechanical sieving and by image analysis or by laser granulometry. Bulk density, porosity, water absorption, thermal conductivity and moisture buffer value are investigated. Finally, the conclusions are drawn and the potential uses of the agro-resources' by-product in building materials are highlighted.

2. Materials and methods
2.1. Materials
This study is performed on five kinds of raw materials with several particle size distributions, collected and processed by CAVAC Company (Vendée, France) in 2015. These raw materials are grown in Vendée.

The bio-based aggregates are processed with an industrial defibering machine by mechanical breaking. In fact, to separate the shiv from the fiber, straw bales are opened, crushed with a hammer mill and sorted into three different categories: fines, fibers and shiv, during the separation process. Only hemp and flax can be changed in fines and fibers. The fines are vacuumed at several process steps. Finally, the shiv are calibrated with different sieving grids (n°7, n°8, n°12 and n°14) using a grader. The uncalibrated shiv go back to hammer mill step (Figure 2).
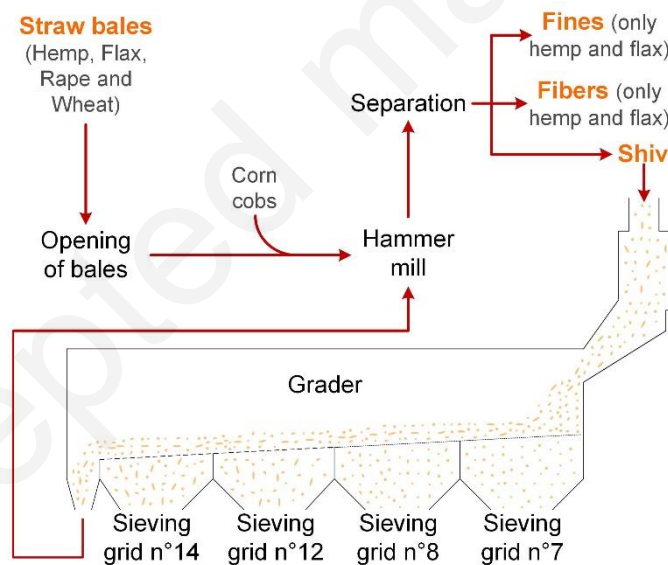

Figure 2: Bio-based aggregates processing flow-chart

The 17 selected bio-aggregates are the following (GX = grid number used to grade the aggregates, Figure 3):
- Hemp shiv (*Cannabis sativa L., Futura 75*): G7, G8, G14 and fines
- Flax shiv (*Linum Usitatissimum L., Angora*): G7, G8, G12, G14 and fines
- Rape straw: G7, G8 and G14
- Wheat straw: G7, G8, G12 and G14
- Corn cobs

The species and variety of rape, wheat and corn are unknown because they are cultivated for their seeds. Therefore, straws or cobs, which are by-products, are mixed without distinctions between variety or species before being sold by the trading industry.

Figure 3: Photos of agro-resources' by-product

2.2. Methods for microstructure characterization
2.2.1. Scanning Electron Microscopy (SEM)
SEM experiments are performed in this study to observe the microstructure of the aggregates. Scanning electron microscopy (SEM) is carried out with a JSM 7100F (Jeol) fitted with Schottky field emission and Everhart-Thornley secondary electron detector.

Prior to the analysis, the aggregates are glued with carbon tape and are coated with palladium (layer thickness average 30 nm) to avoid sample charging effect due to the electron beam.

2.3. Methods for chemical characterization
2.3.1. Fourier Transform InfraRed Spectroscopy (FTIR)
FTIR measurements of raw materials are performed using a Perkin Elmer Spectrum with an ATR-FTIR unit. Without advance preparation, the samples are placed on a crystal (diamond). The spectra are obtained with 10 scans in a spectral range of 650 - 4000 cm^{-1} with a resolution of 4 cm^{-1}. The spectra are collected and analyzed using Spectrum software (Perkin Elmer).

2.3.2. Van Soest Method
The Van Soest method consists in successive extractions to determine the composition of a vegetal sample (Figure 4). The raw materials are crushed and sieved through a 1mm mesh. Then, 500 mg of sample are collected and introduced in porous bag. The first extraction is realized with NDF (Neutral Detergent Fiber) solution, in the ANKOM 2000 Automated Fiber Analyzer at 100°C during 1 hour, to remove soluble cell contents like fat, wax, pectin, proteins and polysaccharides. The remaining fraction contains cellulose, hemicellulose, lignin, and minerals. ADF (Acid Detergent Fiber) solution is used for the second extraction which lasts 1 hour at 100°C, to remove hemicellulose. The remaining fraction contains cellulose, lignin, and minerals. The last extraction is realized with ADL (Acid Detergent Lignin) solution which is 72 % sulfuric acid, in Daisy incubator (Ankom) during 4 hours. During this last extraction, cellulose is solubilized leaving only lignin and

recalcitrant materials. After each extraction, porous bags are rinsed in water and then in acetone. After that, they are dried overnight at 103°C. Then, the calcination of the samples at 550°C for 3 hours leads to the ash content (AFNOR, 1997; Carrier et al., 2011; Contreras et al., 1999; Van Soest et al., 1991).
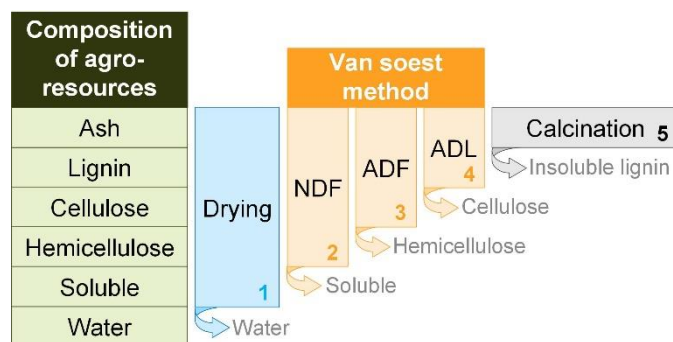

Figure 4 : Synthetic sketch of Van Soest Method allowing accessing the biomass composition (Carrier et al., 2011)

The soluble, cellulose, hemicellulose, lignin and minerals contents of each sample are estimated with these equations (Equations (1) to (5)):

$$\%_{Ash} = \frac{W_{550} - W_{crucible}}{W_{sample} \times \%_{DM}} \tag{1}$$

$$\%_{Lignin} = \%_{ADL} = \frac{W_{ADL} - (W_{bag} \times CC_{ADL}) - (W_{550} - W_{crucible})}{W_{sample} \times \%_{DM}} \tag{2}$$

$$\%_{Cellulose} = \%_{ADF} - \%_{ADL} = \frac{W_{ADF} - (W_{bag} \times CC_{ADF}) - (W_{550} - W_{crucible})}{W_{sample} \times \%_{DM}} - \%_{ADL} \tag{3}$$

$$\%_{Hemicellulose} = \%_{NDF} - \%_{ADF} = \frac{W_{NDF} - (W_{bag} \times CC_{NDF}) - (W_{550} - W_{crucible})}{W_{sample} \times \%_{DM}} - \%_{ADF} \tag{4}$$

$$\%_{Soluble} = \frac{(W_{sample} \times \%_{DM}) + (W_{bag} \times CC_{NDF}) - (W_{550} - W_{crucible})}{W_{sample} \times \%_{DM}} \tag{5}$$

With:
- **W_{sample}:** weight of the sample (mg)
- **$\%_{DM}$:** percentage of dry matter
- **W_{NDF}, W_{ADF} and W_{ADL}:** weight of the sample with the porous bag after the first, second or last extraction (mg)
- **W_{550}:** weight of the sample after the calcination with the crucible (mg)
- **W_{bag}:** weight of the porous bag (mg)
- **$W_{crucible}$:** weight of the crucible (mg)
- **CC_{NDF}, CC_{ADF} and CC_{ADL}:** correction coefficient for the porous bag after the first, second or last extraction

2.3.3. Phenol Sulfuric Method

The phenol sulfuric method consists in total carbohydrate content dosage. Like for the Van Soest method, the raw materials are crushed and sieved through a 1mm square mesh. Then, 3.0 mg of sample are collected and introduced in test tube. After, 9 ml of distilled water, 3 ml of 5 % solution (%w/v) of phenol/water and 15 ml of concentrated sulfuric acid are added. The solution is mixed thoroughly and left for a minimum of 30 minutes. The sulfuric acid causes the hydrolysis of the osidic links and the dehydration of the released monosaccharides to form furfural derivatives which react with the phenol and give the orange color to the solution (Figure 5). The absorbance of the sample solution is measured by a UV-Visible spectrophotometer in the range 550 to 400 nm. The maximum absorbance leads to the sugar content in mg/l from the calibration curve which is established for the range of D(+)xylose (5 - 67 mg/l) (Dubois et al., 1956; Evon, 2008). The amount of color is proportional to the amount of furfural, so the percentage of D(+)xylose is converted to furfural by using a coefficient of 92.5 % (Dubois et al., 1956).
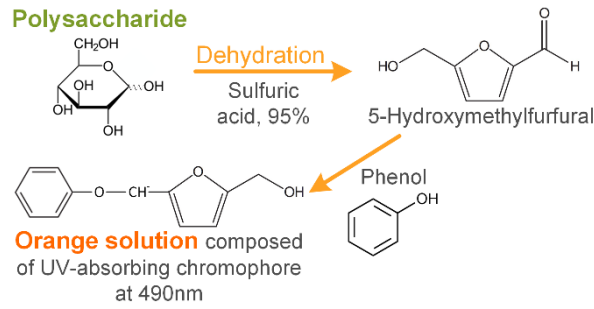
Figure 5 : Schematic overview of the phenol sulfuric method for the total carbohydrate analysis

2.4. Methods for physical characterization
2.4.1. Generality
The physical characterization investigates bulk density, skeleton density, particle's size distribution (PSD), dust content, fiber content, water absorption, thermal conductivity and moisture buffer value (MBV). The open porosity is also calculated from bulk density and skeleton density. The measurement of bulk density, PSD, water absorption and thermal conductivity are based on the recommendations of the Rilem Technical Committee 236 BBM (Bio-aggregate based Building Materials) (Amziane et al., 2017a). The protocol of each measurement is described hereafter.

The bio-aggregates are delivered in big bag. During transport, segregation induces the finest particles to move into the bottom of the big bag. To ensure good representativeness of the sample, the bio-aggregates are homogenized by manual mixing after their reception and at each sampling. For sampling, the homogenized bio-aggregates are put into a pile on a plane and smooth surface. The pile is divided into four similar piles using a non-cutting blade. To obtain the required quantity of sample, the homogenization and division are repeated (Figure 6).

Figure 6 : Sampling method

For measurements performed at dry state, the bio-aggregates are dried in an oven at 60°C until constant mass is reached (variation lower than 0.1 % between two consecutive weighings for three consecutive weighings with a 24-hours time step). Then, they are cooled to ambient temperature in a sealed container. For measurements performed at (23°C, 50 %RH), the bio-aggregates are stabilized in climate chamber until steady state is reached (same criteria as for dry state).

Two kinds of balance are used. For weight higher than 20 g, the used balances are Sartorius LP 8200S and Sartorius LP 4200S. Their readability are 0.01 g, their repeatability are 0.01 g and their linearity are 0.02 g. For weight lower than 20 g, the balance is Sartorius BP 301S. Its readability is 0.0001 g, its repeatability 0.0001 g and its linearity 0.0002 g.

2.4.2. Particle Size Distribution
The Particle Size Distribution is investigated with mechanical sieving for all materials. Image analysis is also performed on shiv and straw and laser diffraction on fines.

2.4.2.1. Mechanical sieving
For mechanical sieving, the sampling is conducted as previously described. The measurement is performed on three 45 $\pm$ 10 g samples (numbered 1, 2 and 3). The mechanical sieving is processed with normative square opening sieves. For shiv and straw, the opening sizes of the sieves are 4, 2, 1, 0.5, 0.25 and 0.1 mm. For Wheat straw G8, G12 and G14, an 8 mm sieve is added. For fines, the opening sizes of the sieves are 2, 1, 0.5, 0.25, 0.16, 0.1 and 0.063 mm. The mechanical

sieving is performed with a mechanical sieve shaker. The vibration duration is 20 minutes. The weighing of each sieve with and without aggregate leads to the retained mass fraction on each sieve. It is checked that the sum of the retained mass corresponds to the initial input mass of material. The passing masses are then calculated. According to the Construire en Chanvre recommendation for shiv characterization, the dust content of shiv is equal to the passing at 0.25 mm.

2.4.2.2. Image analysis

The image analysis is performed on 6 grams samples. It is checked that they include at least 2000 identified particles. If not, other 6 grams samples are added up to reach the required number of particles. A flatbed scanner is used, avoiding image distortion and ensuring repetitive calibration. The acquired images are 8-bit grey scale with 600 DPI resolution. The particles are spread in a manner that they do not touch or overlap one another. A dark background is used in order to have the maximum contrast. The analysis is performed with Image J. The particles are fitted with ellipses (same area and centroid as particle, Figure 7). The minimum Feret's diameter gives the width w of the particle while the maximum Feret's diameter of ellipse gives the length l (Picandet et al., 2012). The ε elongation ratio is the ratio of length to width (l/w). The PSD is calculated from two-dimension image analysis, considering quasi-homothetic particle shape and quasi-constant density of particles. The mass distribution of particles is thus calculated from the projected area A_i and the width w_i of the particles according the following equation (6):

$$P_m(X \leq x_n) \cong \frac{\sum_{i=1}^{n} A_i \times w_i}{\sum_{i=1}^{N} A_i \times w_i} \tag{6}$$

The Rilem TC BBM advises performing the analysis on the range 0.18 mm² to infinity. The sieving method shows that studied aggregates include smaller particles (0.25 mm passing). The analysis is thus performed on the range 0.06 mm² to infinity.

During the spreading of samples, the fibers are collected to quantify the fiber content which is the ratio of fiber mass to sample mass.

Figure 7: Image processing from left to right: scan, binarization of the image, grayscale conversion and ellipses fitting

2.4.2.3. Laser diffraction particle sizing

The particle size distribution of fines is also measured by laser diffraction using the Malvern Mastersizer 2000 apparatus with the Scirocco 2000 dry dispersion unit. This measurement is based on the principle that particles passing through a laser beam scatter light at an angle that is directly related to their size. The laser diffraction leads to the diameter of the sphere with the same volume of the particle. The distribution is given in volume ratio. The particle size ranges from 0.02 µm to 2000 µm.

2.4.3. Bulk density

The bulk density is measured at dry state and at (23°C, 50 %RH). The measurement is performed with a transparent plastic cylinder, 94 mm in diameter and 204 mm in height. The aggregates are poured into the cylinder. Their quantity is chosen to fulfill about half the volume of the container. The cylinder is upended ten times to ensure representativeness of bulk aggregates. The whole is slightly shaken to obtain a horizontal level, which is marked using a cardboard disc. The mass of shiv is calculated from the cylinder weightings (without and with aggregates). The volume is calculated by weighing the cylinder filled with water up to the marked level. The bulk density is then the ratio of the mass to the volume. The accuracy of the measurement is calculated from the characteristics of the balance and from the accuracy of the level, estimated about 0.5 mm. This accuracy is better than 1 %. For each material, the measurement is repeated five times.

2.4.4. Skeleton density

The skeleton density is measured with a manual pycnometer. The dry aggregate is put into the pycnometer. It is then immersed in toluene and regularly shaken until no bubbles can be seen. The pycnometer is then totally filled with toluene. Successive weightings of pycnometer, pycnometer with dry aggregates, pycnometer with aggregates filled with toluene and pycnometer filled with water leads to the mass of aggregates and to their volume. The density of toluene is also measured with pycnometer, filling it with toluene on the one hand and with water on the other hand. One pycnometer is used for each material. For hemp shiv, rape straw, flax shiv and hemp and flax fines, the volume of pycnometer is about 600 ml. For wheat straw, the volume of the pycnometer is about 1200 ml (ASTM International, 1997).

2.4.5. Water absorption

The protocol to measure water absorption is based on the recommendations of the Rilem TC BBM (Amziane et al., 2017a). The measurement is performed using water permeable bag and salad spinner. Around 20 g of dry aggregates are used for each sample. After wetting, the bag (without or with sample) is spun at 195 rounds in one minute before weighing. The aim of the spinning is to eliminate water adsorbed at the surface of particles or located between particles. A first measurement is performed on empty bag (Figure 8).
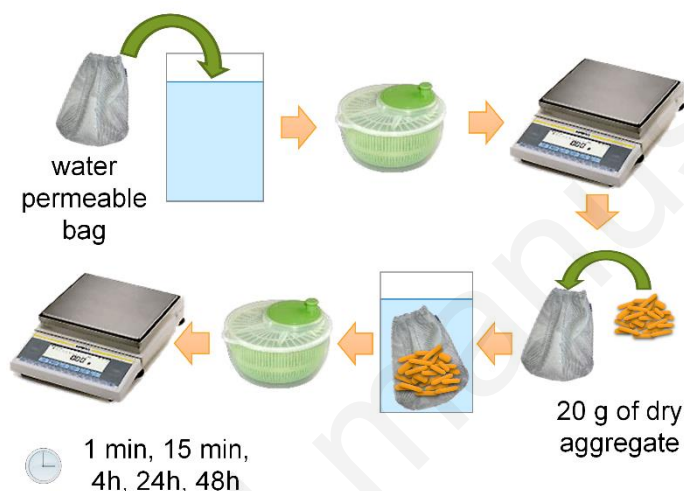

Figure 8 : Protocol to measure water absorption

The weight of wet sample is calculated from the weight of bag with wet sample and of empty bag. The measurement is performed after one minute, 15 minutes, 240 minutes, 1440 minutes and 2880 minutes. At each time, the water content of the sample is calculated with equation (7).

$$w(t) = \frac{m(t) - m_0}{m_0}$$

(7)

Where m(t) is the mass of the wet sample at t time (g), m_0 is the mass of the dry sample (g).
The variation of water content with time is then fitted with:

(8)

$$w(t) = IRA + K_1 \times \log(t)$$

Where IRA is the Initial Rate of Absorption which characterizes external water adsorption and K_1 is the slope of the curve of water content versus logarithmic time which corresponds to a kind of diffusion rate. The correlation coefficient R^2 qualifies the quality of the fitting.

For each aggregate, the measurement is performed on three samples. Then, the IRA and the K1 values are averaged to lead to the characteristic curve of the aggregate. The standard deviation is also calculated to indicate the repeatability of the measurement.

2.4.6. Thermal conductivity

The thermal conductivity is measured on bulk aggregate, at 23°C and dry state. The measurement is performed with a hot wire following the recommendation of the Rilem TC BBM (Amziane et al., 2017a). The device consists of two containers filled with bulk aggregates. The sensor is embedded between the two containers (Figure 9). The sensor used is a five centimeter long hot wire. The heat flow and heating time are chosen to reach high enough temperature rise (>10°C) and high correlation coefficient (R^2) between experimental data and fitting curve given equation (9). The heating power is 0.142 W and the heating time is 90 s.

$$\Delta T = \frac{q}{4\pi\lambda}(ln(t) + K) \tag{9}$$

where q is the heat flow per meter (W.m^{-1}) and K is a constant including the thermal diffusivity of the material. The sensor is regularly checked by measuring thermal conductivity of reference material which thermal conductivity is 0.039 W/(m.K). The containers allow to control the bulk density of aggregate. Their size is chosen to be high enough to ensure that heat flux remains in the sample. Their diameter is twice the length of the sensor. Each container is thus 10 centimeters in diameter and 7.5 cm in height. When the sample is prepared, its bulk density is checked to ensure representativeness of the material. The upper side of the top container is covered with a plate to prevent any moisture exchange during measurement. The measurement of thermal conductivity is repeated 5 times for each material. According to the manufacturer, the hot wire is well adapted for the measurement of thermal conductivities ranging from 0.02 to 5 W.m^{-1}.K^{-1} and the expected accuracy is 5 %.

Figure 9: Experimental device for the measurement of thermal conductivity

2.4.7. Moisture Buffer Value

The moisture buffer value MBV quantifies the ability of materials to moderate the variations of ambient relative humidity. It is measured following the NORDTEST project method (Rode et al., 2005). This value relates the amount of moisture uptake (and release), per open surface area, under daily cyclic variation of relative humidity as shown in the following equation:

$$MBV = \frac{\Delta m}{A \times \left(RH_{high} - RH_{low}\right)} \tag{10}$$

Where MBV is the Moisture Buffer Value (g/(m².%RH)), Δm is the moisture uptake / release during the period (g), A is the open surface area (m²) and $RH_{high/low}$ are the high/low relative humidity level (%).

Within the NORDTEST project, a round robin test was performed on nine representative building materials. It gives initial results and leads to a classification of moisture buffer values from negligible to excellent (Figure 10).
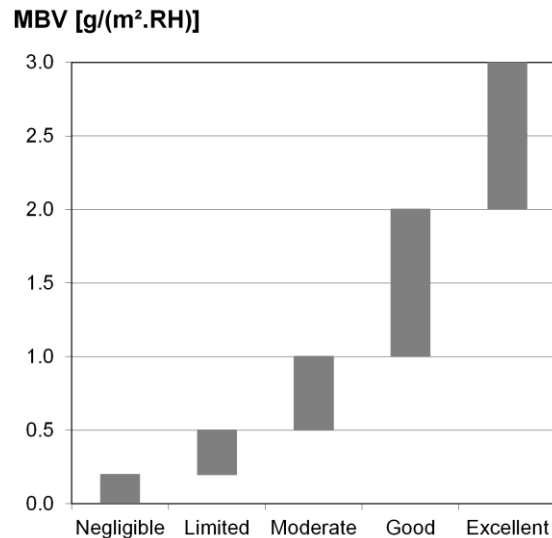
Figure 10: Nordtest project classification of materials versus Moisture Buffer Value

In this study, the samples are put in containers of about 12 cm in diameter. The volume of the samples is about 800 to 1000 cm³. The average horizontal air velocity in the surroundings of the exchange surface is 0.07 m/s, which meets the requirements of the Nordtest Project protocol.

3. Results and Discussions
3.1. Microstructure characterization

Figure 11 shows the longitudinal and cross sections with different magnifications of the agro-resources by-product and highlights a very porous structure. Table 2 summarizes the microstructure: tissue layers, cells type and cells size, of agro-resources' by-products. The agro-resources' by-products have different micro-structures due to the following reasons:

- Depending on the plant part used as aggregates, the structure differs. Therefore the corn cob, which is not a stem like other raw materials, have a different structure;
- Depending on the plant growth, the cells size differs as well as the number of layers and their composition. The growth depends on the time and the season of growth, of flowering or of harvest, on the weather and on the soil composition.
- Depending on the aggregates processing, given cellular layers can be removed or not from the raw material. For hemp and flax, the industrial defibering machine allows the separation of the shiv from the fiber, and thus, the epidermis is not a layer of these shiv.

The plant's body is made up of 3 types of tissues, which have a variety of functions, and which are the followings (Amziane et al., 2017b; Taiz and Zeiger, 2002; Vignon et al., 1995):

- Dermal tissue, in other words the epidermis (outer most layer for protection);
- The vascular tissue system: xylem (transport water) and phloem layers (transport food);
- The ground tissue: made up of parenchyma (food storage), of collenchyma (mechanical support) and of sclerenchyma cells (mechanical support and protection, fiber).

The epidermis (Ep) is the boundary between the plant and the outside world. It provides protection and regulates exchanges (gas, water, mineral nutrients …) with the surrounding environment. It is coated with a waxy cuticle on its outer layer to prevent water loss. Figure 11 h, k and o show some epidermis cells as well as the cuticle. In the case of corn cobs, the silk is also visible on outer surface (Figure 11 o).

The phloem layer (PL) transports sugars, proteins and minerals. It may contain the following type of cells: sieve tubes (ST), sclerenchyma and parenchyma cells (PC). The ends of the sieve tubes are perforated by sieve plates, and sap passes through the sieve plates from one sieve tube member to another. Figure 11 a, c, h, j, k, m, n and o show the phloem layer

for each agro-resource, with the sieves tubes and the parenchyma cells. In Figure 11 a, m and n, the parenchyma cells contain the starch granules (Cortella and Pochettino, 1994).

The vascular cambium (VC) is a plant tissue located between the xylem and the phloem layers. When it grows, it forms a ring which is known as cambium ring. Figure 11 c shows the vascular cambium in the case of the hemp shiv.

The xylem layer (XL) transports water and is composed of two types of cells: tracheids (Tr) and vessel (Ve). Both cells are dead when mature. Tracheids are long and pitted cells to allow the water to pass. These cells are visible, on Figure 11 b, d, e, f, g, h, j, k and l, for all agro-resources except the corn cobs. Vessels have a larger diameter but a shorter length than tracheids and their end walls have disappeared in order to form a continuous series of tubes. The efficiency of water flow is better than in the tracheids. The secondary wall thickenings of vessels may be annular, spiral, scalariform, reticulate or pitted. Figure 11 b, g, h, j and k show the vessels of hemp shiv, rape and wheat straw.

The largest parenchyma cells composed the pith (Pi) layer. Figure 11 i shows the pith cells in the rape straw.
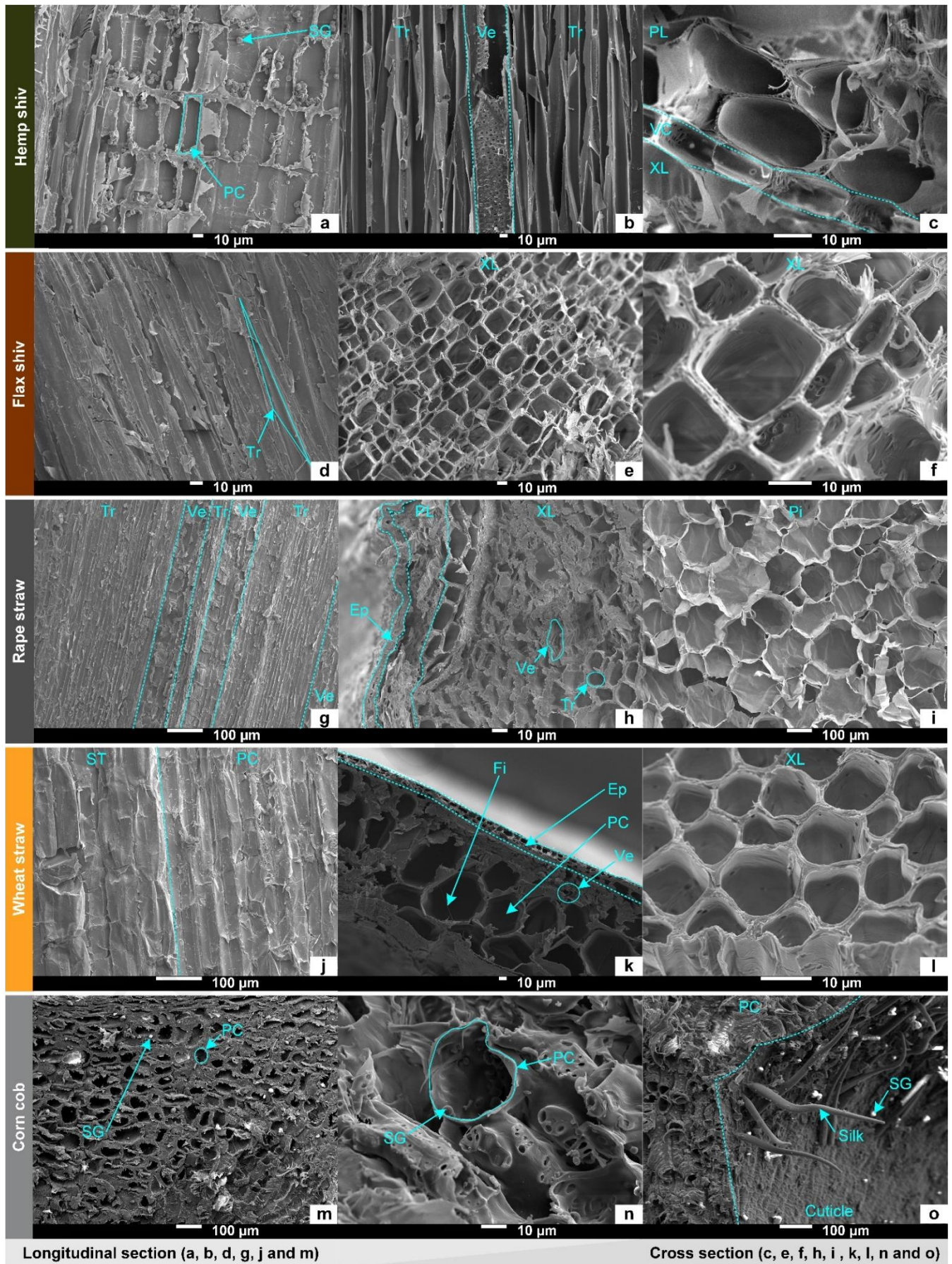
Figure 11: Longitudinal and cross sections of agro-resources' by-product (Ep: epidermis, Fi: Fiber, PL: phloem layer, PC: parenchyma cell, ST: sieve tube, SG: starch granule, VC: vascular cambium, XL: xylem layer, Tr: tracheid, Ve: vessel, Pi: pith and HS: hollow space)

Table 2: Micro-structure of agro-resources' by-product and properties of their tissue layers (cells type and size)

		Epidermis (Ep)	Phloem layer (PL)			Vascular cambium (VC)	Xylem layer (XL)		Pith (Pi) or Hollow space (HS)	Micro-structure
			Parenchyma cells (PC)	Sieve tubes (ST)	Starch granules (SG)		Tracheids (Tr)	Vessels (Ve)		
Hemp shiv	**Type**	Rectangular	-	-	Spherical (simple or compound)	Rectangular	Pitted	Annular	Hollow space	(Bouloc, 2006)
	Ø (µm)	l_1 : 6 - 8 l_2 : 10 - 12	10 - 20	35 - 50	3 - 7	l_1 : 6 - 8 l_2 : 14 - 18	10	50		
	L (µm)	-	50 - 70	-	-	-	100 - 150	90 - 110		
Flax shiv	**Type**						Pitted	Reticulate	Hollow space	(Johnson and Kerr, 2015)
	Ø (µm)	Purposeless	Purposeless			Purposeless	9 - 12	15 - 35		
	L (µm)						130 - 150	-		
Rape straw	**Type**		-	-	Spherical (simple)		Pitted	Reticulate	Pith	
	Ø (µm)	Not measurable	10 - 20	-	3 - 5	Not observed	10	15 - 50	50 - 100	
	L (µm)		130	-	-		100 - 130	30 - 50	-	
Wheat straw	**Type**	Rectangular	-	-	Spherical (simple)		Pitted	Annular	Hollow space	(Ghaffar, 2017)
	Ø (µm)	l_1 : 5 - 8 l_2 : 10 - 12	5 - 25	50	20	Purposeless	6 - 15	25 - 30		
	L (µm)	-	160 - 220	100	-		-	-		
Corn Cob	**Type**		Polyhedral	-	Polyhedral (simple)				Not observed	(Pinto et al., 2012)
	Ø (µm)	Purposeless	40	-	5	Purposeless	Purposeless			
	L (µm)		100	-	-					

Figure 12 shows the inside surface of rape straw, outside and inside surfaces of wheat straw and outside surface of corn cobs, with different magnifications. The pith layer of rape straw is visible on Figure 12 a and b. Indeed, it composes the inside surface of the straw after its crushing which induces damage. Outside surface of wheat straw is visible on Figure 12 c. The cuticle of the wheat straw has a flat surface. Inside surface of wheat straw is visible on Figure 12 d. The surface is

flat and includes starch granules (SG) and recrystallized starch (RS) (Pérez and Bertoft, 2010). Figure 12 e and f show the outside surface of corn cobs. The cuticle is smooth between the "rope-like" upwellings (Graaff and van Staden, 1983). It also includes starch granules.
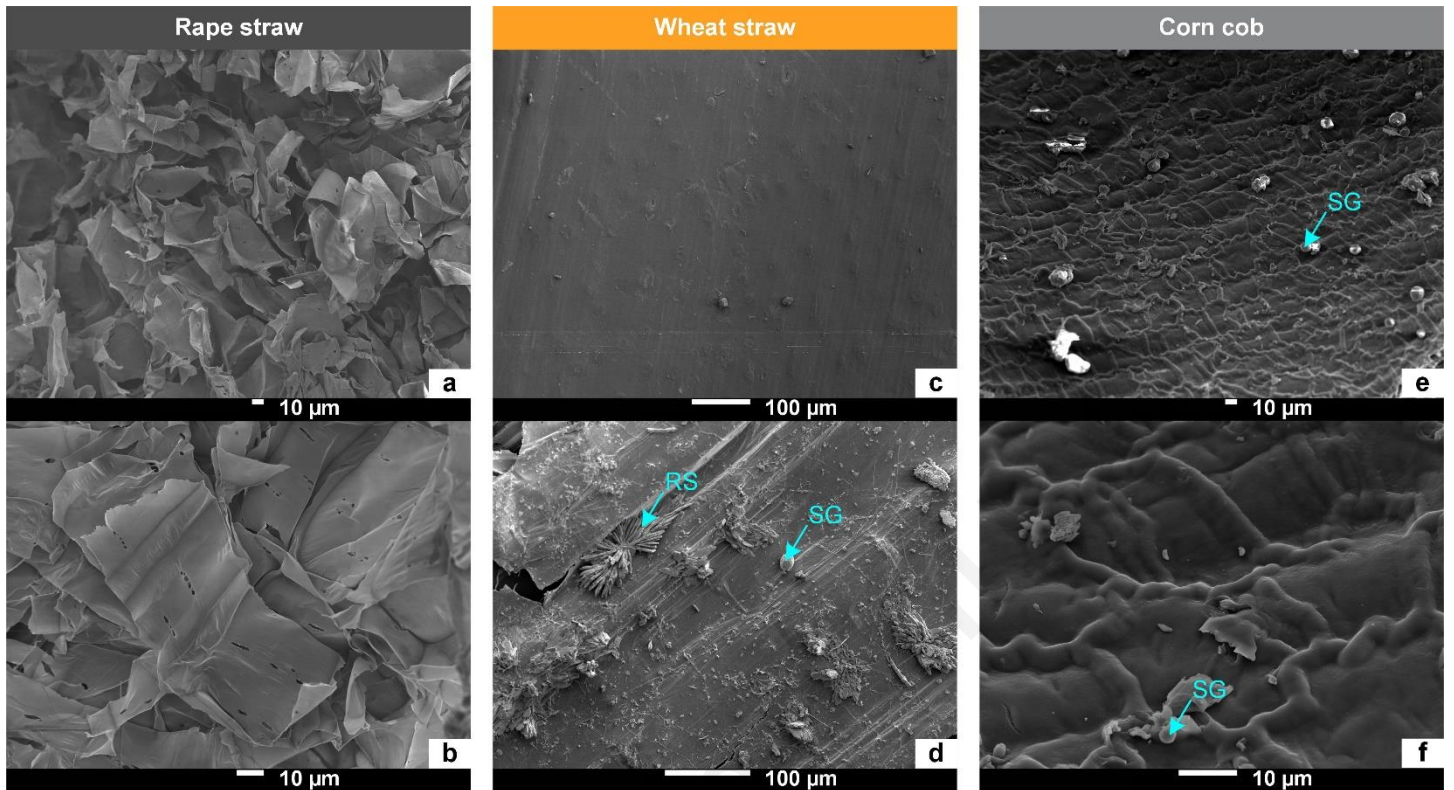

Figure 12: Inside surfaces (a, b and d) and outside surfaces (c, e and f) of agro-resources' by-product (SG: starch granule and RS: recrystallized starch)

Figure 13 shows the hemp and flax fines with different magnification. Table 3 summarizes the particles type of hemp and flax fines, including their size. The fines are composed of shiv, fibers and dust. The shiv are smaller than 3 mm. The fibers have a diameter around 10 µm and a length higher than 1500 µm for hemp and higher than 3000 µm for flax. Figure 13 c and f show the structure of a dust which is a crushed shiv. Indeed on the SEM micrographs, the spiral vessel (for hemp) or reticulate vessel (for flax) and pitted tracheids, which are the part of the xylem layer, are visible.
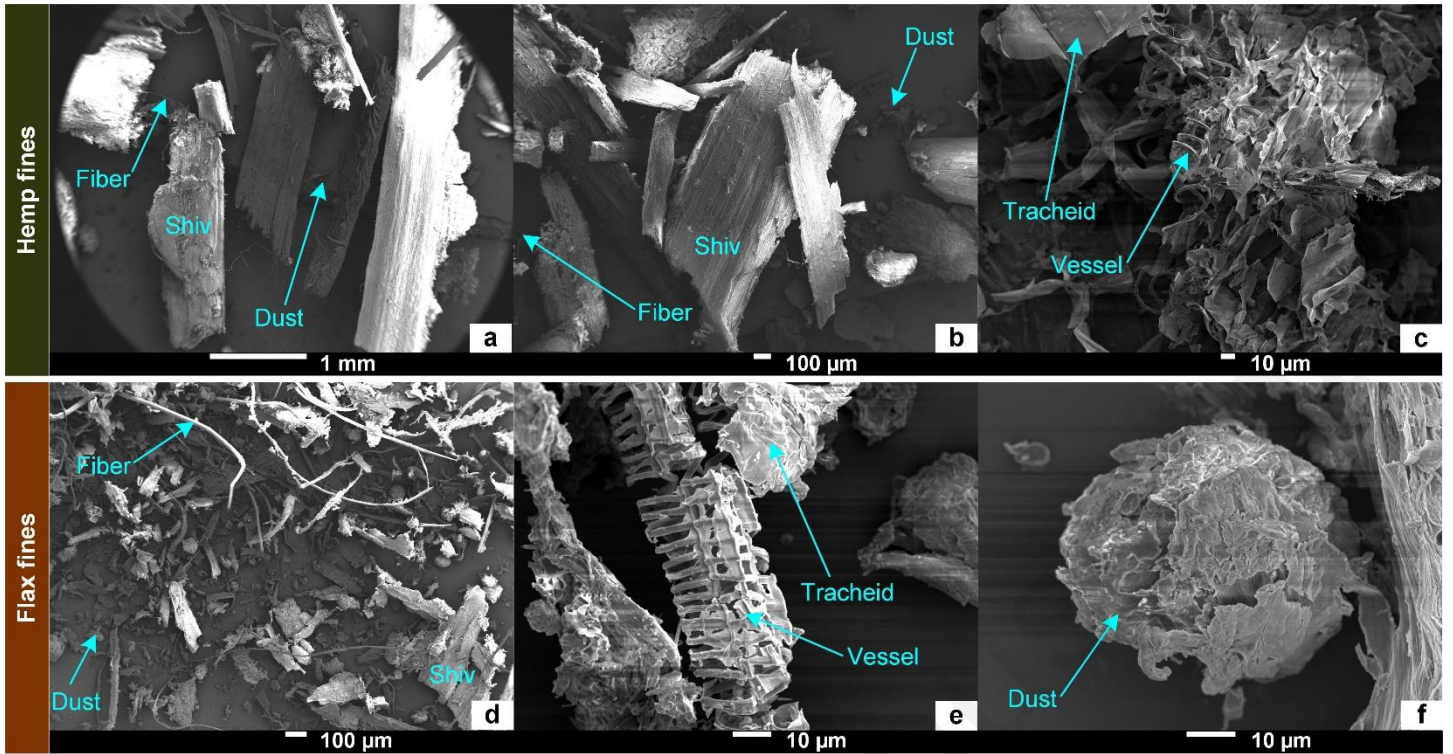
Figure 13: SEM micrographs of hemp and flax fines

Table 3: The particles type and their size composing the hemp and flax fines

	Shiv	Fiber	Dust
Hemp fines	< 3 mm	Ø : 10 µm L : 1500 µm	< 0.25 mm
Flax fines	< 3 mm	Ø : 10 µm L : 3000 µm	< 0.25 mm

3.2. Chemical characterization

Figure 14 gives the FTIR spectra of shiv and straw from agro-resources' by-products while Table 4 gives a bibliographic review of assignments of FTIR absorption bands. The cellulose spectrum has one distinct peak at wavenumbers of 719 cm^{-1}. The lignin spectrum shows characteristic peaks at wavenumbers around 3300, 1638, 1583, 1512, 1463 and 1095 cm^{-1}. The hemicellulose spectrum has characteristic peaks at wavenumbers around 2918, 1734, 1415, 1371, 1240, 1150, 1019, 954 and 895 cm^{-1}. However, the hemicellulose does not have specific bonding, and thus specific wavenumber, corresponding to itself. Indeed, the monomers structure composing the hemicellulose are similar to the cellulose units, to the pectin monomers or to the lignin monomers as shown in Figure 12. More, the FTIR detects only an atomic grouping thanks to their characteristic frequency of vibration and not a molecule.

Studied agro-resources show similar spectra with these characteristic peaks. For a given peak, the intensity depends on agro-resource. For all of them, the main peak is at 1031 cm^{-1}, characteristic of cellulose, lignin, hemicellulose and pectin. From observed peak, four main components may be identified: cellulose, lignin, hemicellulose and pectin. However, absorption bands may fit several components. Therefore, this chemical characterization technic allows to affirm the presence of cellulose and lignin only.
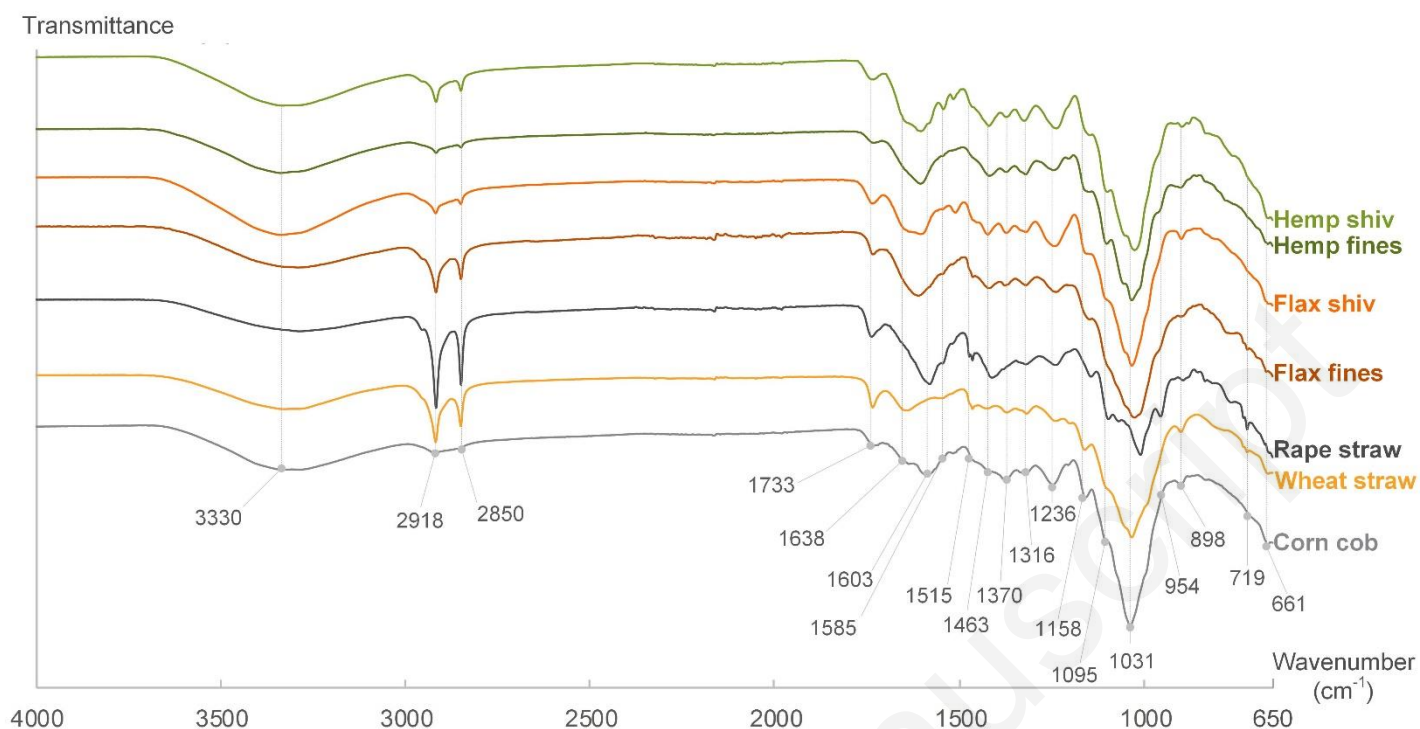
Figure 14: FTIR spectra of agro-resources' by-product

Table 4: Assignments of FT-IR absorption bands (cm^{-1})

Absorption bands (cm^{-1})	Assignments	Source	References
3291 - 3336	O-H stretching	lignin, polysaccharides	(Terpáková et al., 2012; Xu et al., 2006, 2013; Zhang et al., 2015)
2917 - 2918	C-H stretching of methyl, methylene or methane group	cellulose, fat, hemicellulose, polysaccharides, wax	(Terpáková et al., 2012; Xu et al., 2006, 2013)
2849 - 2850	CH_2 asymmetrical and symmetrical stretching	fat, lignin, polysaccharides, wax	(Abidi et al., 2014; Terpáková et al., 2012; Xu et al., 2013)
1731 - 1737	C=O unconjugated stretching acetyl groups	lignin, xylan (hemicellulose)	(Abidi et al., 2014; Diquélou et al., 2015; Manara et al., 2014; Terpáková et al., 2012; Xu et al., 2006, 2013)
1638	OH bending of adsorbed water C=O stretch in conjugated ketone	water lignin	(Abidi et al., 2014; Terpáková et al., 2012; Xu et al., 2006)
1603	aromatic skeletal vibrations	lignin	(Manara et al., 2014; Xu et al., 2006)
1579 - 1588	aromatic ring vibration, C=O stretch and stretching	lignin	(Xu et al., 2013)
1509 - 1515	C=C aromatic symmetrical stretching	lignin	(Manara et al., 2014; Terpáková et al., 2012; Xu et al., 2006, 2013)
1463	C=C aromatic symmetrical stretching Aromatic methyl group vibrations	lignin	(Manara et al., 2014; Terpáková et al., 2012; Xu et al., 2006)
1411 - 1421	aromatic skeletal vibrations	hemicellulose, lignin, pectin	(Abidi et al., 2014; Manara et al., 2014; Xu et al., 2006, 2013)
1370 - 1373	aliphatic C-H stretch in CH_3	cellulose, hemicellulose, lignin, polysaccharides	(Abidi et al., 2014; Xu et al., 2006, 2013)
1316 - 1323	C–O stretching	cellulose, syringyl (lignin)	(Xu et al., 2006; Zhang et al., 2015)

|			
1236 - 1245	aromatic C–O stretching	lignin, xylan (hemicellulose)	(Abidi et al., 2014; Diquélou et al., 2015; Manara et al., 2014; Xu et al., 2006; Zhang et al., 2015)
1142 - 1159	C–O stretch in ester groups	cellulose, hemicellulose, lignin	(Abidi et al., 2014; Manara et al., 2014; Xu et al., 2006; Zhang et al., 2015)
1095 - 1098	aromatic C-H in-plane deformation	guaiacyl (lignin)	(Abidi et al., 2014; Xu et al., 2006)
1008 - 1036	C-C, C-OH, C-H ring and side group vibration	cellulose, hemicellulose, lignin, pectin	(Abidi et al., 2014; Terpáková et al., 2012; Xu et al., 2013; Zhang et al., 2015)
954	glycosidic bonding	cellulose, hemicellulose	(Xu et al., 2013)
892 - 899	β-glycosidic bonds symmetrical ring-stretching mode	hemicellulose, polysaccharides	(Abidi et al., 2014; Terpáková et al., 2012; Xu et al., 2013)
719	CH$_2$ rocking	cellulose	(Abidi et al., 2014)
661 - 663	O-H out-of-plane bending	cellulose, polysaccharides	(Abidi et al., 2014; Terpáková et al., 2012)
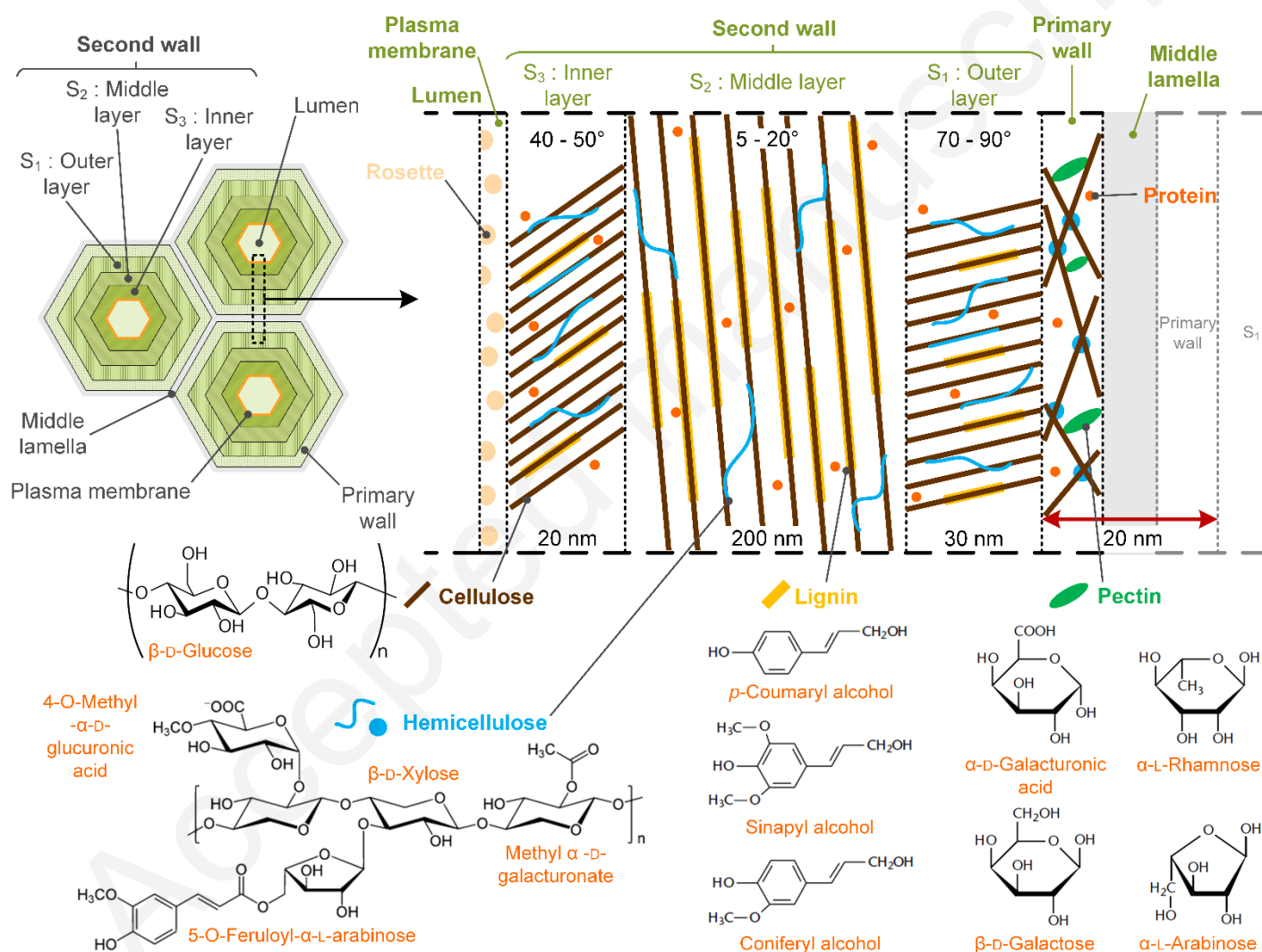
Figure 15: Diagrammatic illustration of the cell plant based on references (Anwar et al., 2014; Harris, 2006; Sorieul et al., 2016) for the cell wall model and references (Anwar et al., 2014; Fry, 2001) for the chemical composition

The Van Soest method allows quantifying cellulose, hemicellulose, lignin, soluble and ash in agro-resources' by-products. The results are shown in Table 5. Soluble is mainly composed of pectin, protein and lipid (fat and wax). Large differences in the chemical composition between these raw materials are evident. On a dry-weight basis, agro-resources' by-products contain 55 – 95 % of polysaccharides (cellulose, hemicellulose and pectin). The cellulose is the most abundant component in the plant cell, except in the case of the corn cob where it is hemicellulose. According to Figure 15, it makes sense. Indeed,

this component is present in all the different walls of plant cell, in the form of cellulose microfibrils (fiber-like strand), randomized in the primary wall and then in parallel of varying inclination according to the layer of the second wall. Cellulose microfibrils has a rigid structure, formed from many cellulose molecules, in order to create the strong support structure that allows agro-resources to stand upright. Between the cellulose microfibrils, hemicellulose forms network and is the second component of plant cells. In the second wall, lignin which is the second most abundant polymeric organic substance in plant cell wall, acts as a cement. It has a supportive structural function and also protects the cellulose and hemicellulose (Chen, 2014; Sorieul et al., 2016).

Corn cob has the lowest lignin and ash content (3.30 % and 0.46 %) but the highest hemicellulose content (38.81 %). Flax fines have the lowest hemicellulose and cellulose contents (15.80 % and 28.51 %) but the highest soluble and ash content (29.15 % and 4.20 %). Flax shiv has the lowest soluble content (7.56 %) but the highest lignin content (20.98 %). Rape straw has the highest cellulose content (53.06 %).

Table 5: Chemical composition of agro-resources by the Van Soest method

Agro-resources	Cellulose (%)	Hemicellulose (%)	Lignin (%)	Soluble (%)	Ash (%)
Hemp shiv	49.97 ± 0.81	21.42 ± 0.71	9.52 ± 0.11	17.75 ± 0.51	0.67 ± 0.02
Hemp fines	42.66 ± 1.45	18.87 ± 0.57	11.52 ± 0.37	23.93 ± 1.89	1.62 ± 0.22
Flax shiv	44.63 ± 0.64	24.41 ± 0.64	20.98 ± 0.21	7.56 ± 0.66	1.48 ± 0.16
Flax fines	28.51 ± 0.79	15.80 ± 0.26	18.14 ± 0.28	29.15 ± 0.35	4.20 ± 0.07
Rape straw	53.06 ± 0.57	18.13 ± 0.59	9.63 ± 0.32	17.68 ± 0.81	0.79 ± 0.07
Wheat straw	43.04 ± 0.16	29.66 ± 0.86	5.24 ± 0.01	20.43 ± 0.78	0.82 ± 0.02
Corn cob	36.78 ± 0.96	38.81 ± 0.72	3.30 ± 0.10	19.30 ± 1.74	0.46 ± 0.01

Table 6 summarizes values found in the scientific literature. For a given agro-resource (same variety and species) discrepancies appear as well as in bibliography review as between this study and bibliography. Indeed, the chemical composition also depends on the area of production, the weather (sunlight, relative humidity, temperature, rainfall and wind) and the maturity of the plant (Kymäläinen and Sjöberg, 2008; Vignon et al., 1995). Agro-resources adapt to the environment in which they grow. Generally speaking, agro-resources from CAVAC (Vendée, France) contain less lignin and ash, and are more soluble compared to the composition of lignocellulosic biomass resources in the scientific literature. However, these results are in the range of the bibliography review.

Table 6: Chemical composition (cellulose, hemicellulose, lignin, soluble and ash) of agro-resources based on the scientific literature

Agro-resources	Cellulose (%)	Hemicellulose (%)	Lignin (%)	Soluble (%)	Ash (%)	Ref.
Hemp shiv (Cannabis sativa L., LCDA - France)	44.00	18.00	28.00	8.00	2.00	(Vignon et al., 1995)
Hemp shiv (Cannabis sativa L., Futura, Italy)	51.60	21.50	12.90	12.90	6.60	(Cappelletto et al., 2001)
Hemp shiv (average on 15 references)	47.50 ± 3.50	6.40 ± 1.50	8.00 ± 1.00	29.40 ± 3.60	8.80 ± 1.00	(Godin et al., 2010)
Flax shiv (Canada)	38.06 ± 0.57	25.03 ± 0.57	31.20 ± 0.22	4.00 ± 0.27	1.71 ± 0.05	(Ross and Mazza, 2010)
Flax shiv (Linum Usitatissimum L.)	53.00	13.00	24.00	1.50	> 2 %	(Sain and Fortier, 2002)
Rape straw (Poland)	37.55	31.37	21.30	3.76	6.02	(Greenhalf et al., 2012)
Wheat straw	38.60	32.60	14.10	-	5.90	(Sun and Tomkinson, 2000)
Corn cob (average on 10 species - Austria)	38.80 ± 2.50	44.40 ± 5.20	11.90 ± 2.30	5.21 ± 1.1	2.88 ± 0.11	(Pointner et al., 2014)

Table 7 gives the pectin content of studied agro-resources determined by phenol-sulfuric method. Pectin is complex macromolecule, as it can be composed of as many as 17 different monosaccharides containing more than 20 different

chemical bonds (Figure 15). Pectin is present, in the cell plant, in the middle lamella, primary walls and second walls. Pectin plays several roles in the growth plant period: it lends strength and supports to the plant, it activates plant defense responses, and it induces a lignification (Voragen et al., 2009). Following Table 7, for each agro-resource, pectin is the main component of soluble. For flax shiv, rape straw, wheat straw and corn cob, the quantity of pectin, obtained by phenol-sulfuric method, is higher than the quantity of soluble measured with Van Soest method. This is due to pectin extraction process. Indeed, cold water allows to solubilize pectin and part of hemicellulose but no cellulose (Gao et al., 2014; Silva et al., 2014). Flax shiv is the bio-based aggregates which has the biggest difference between the quantities of pectin and soluble, it's also the agro-resource which has the highest quantity of lignin. More, in Van Soest method, the lignin is removed with 72 % sulfuric acid at room temperature. In the phenol sulfuric method, the lignin is not removed. It reacts to form chromophore (Dyer, 1999) which interacts with those of phenol sulfuric method. So, with the hypothesis that 50 % of lignin react with sulfuric acid, the quantity of pectin is corrected by subtracting 50 % of lignin's content to the measured quantity of pectin. After this correction, the corrected pectin to soluble ratio seems consistent. There are always very few protein and lipid (soluble without pectin) except for hemp shiv and flax fines. The cell wall surfaces of the epidermic cell are covered with cutin and suberin (lipids) to reduce water loss from the plants (Chen, 2014). Proteins provide carbon, nitrogen, and sulfur resources for subsequent growth and development of the plant (Herman and Larkins, 1999).

Table 7: Content of pectin in agro-resources' by-product

Agro-resources	Pectin (%)	[Pectin] / [Soluble] (%)	Corrected Pectin (%)	[Corrected Pectin] / [Soluble] (%)
Hemp shiv	13.95 ± 0.36	78.59	9.19	51.77
Hemp fines	17.28 ± 6.70	72.21	10.22	42.72
Flax shiv	17.19 ± 0.93	227.44	6.71	93.20
Flax fines	17.48 ± 1.13	59.96	8.41	28.85
Rape straw	19.34 ± 0.83	109.41	14.53	82.15
Wheat straw	20.58 ± 1.46	100.73	17.96	87.92
Corn cob	19.99 ± 0.57	103.60	18.34	95.05

In Table 8, these values are compared with these in the scientific literature. For hemp shiv and corn cob, agro-resources from CAVAC (Vendée, France) contain more pectin compared to the composition of lignocellulosic biomass resources in the scientific literature. For hemp shiv, the proportion between pectin, protein and lipid are the similar. For rape straw, agro-resource from CAVAC (Vendée, France) contains less pectin and more protein and lipid compared to the composition of lignocellulosic biomass resources in the scientific literature. Like for the content of cellulose, hemicellulose, lignin, soluble and ash, the compositions differ because of the area of production, the weather and the maturity of the plant (Kymäläinen and Sjöberg, 2008; Vignon et al., 1995).

Table 8 : Content of pectin, protein and lipid in agro-resources based on the scientific literature

Agro-resources	Pectin (%)	Protein (%)	Lipid (%)	Reference
Hemp shiv (Cannabis sativa L., LCDA - France)	4.00	3.00	1.00	(Vignon et al., 1995)
Rape straw (Korea)	19.40 ± 0.50	1.60 ± 0.10	-	(Jeong and Oh, 2011)
Corn cob (average on 10 species - Austria)	0.67 ± 0.12	4.26 ± 0.96	0.30 ± 0.02	(Pointner et al., 2014)

3.3. Physical characterization
3.3.1. Particle size distribution, dust content and fiber content
Figure 16 gives an example of raw data obtained on hemp from image analysis. Figure 17 to Figure 21 give the particle size distributions obtained from mechanical sieving and from image analysis (width and length) for hemp shiv, flax shiv, rape straw, wheat straw, corn cob respectively. Figure 22 gives the particle size distributions obtained from mechanical sieving and from laser diffraction particle sizing (radius) for hemp and flax fines.

Table 9 and

Table 10 summarize the particle size distribution analysis, the dust content and the fiber content.

Globally, the particle size (width and length) increases with the grader grid number. For flax, the width are nearly the same, whatever the length of shiv. For hemp and rape, G7 shiv are smaller than G8 which are smaller than G14. For flax and wheat, the length of G8 shiv is smaller than the length of G7 shiv but the width is higher. This may be due to that to pass through the grid, the shiv need to be smaller than the grid both in length and in width. So, G8 shiv show higher width than

G7 shiv despite their length is smaller. For wheat straw, G14 is smaller than G12, both in width and length. Wheat straw being flexible, maybe it is distorted under grader's effect and charge due to other straw. So, bigger straw can pass through smaller grid.

For small particles (G7 and G8), the length of hemp and flax are close, both in L_{10}, L_{50} and L_{90}. Rape shows slightly higher length and wheat is longer. For big particles (G12 and G14), the smallest particles are G12 and G14 flax shiv ($L_{90}=16.753$ and 18.495 mm respectively), the biggest ones are G12 wheat straw ($L_{90}=39.022$ mm). G14 hemp shiv and G14 wheat straw are close (L_{90} about 30 mm), G14 rape straw is slightly smaller ($L_{90}=27.270$ mm).

The particle size distributions obtained for hemp shiv are in the range of PSD found in bibliography (Table 11). The results obtained for G7 and G8 hemp shiv are particularly close to the results of S2 Hemp shiv in (Arnaud and Gourlay, 2012) and of "Chanvre d'Auvergne" in (Nozahic et al., 2012). Indeed, the PSD mainly depends on the production process, more specifically number of hammer mills, quality of separation and vacuum of fines.

For shiv and straw, the medium elongation ratio ranges from 3.052 to 9.482. Whatever the agro-resource, the elongation ratio increases with the length of shiv. Hemp shiv and rape straw show the smallest elongation ratios (from 3 to 5.1 for medium value). Flax shiv show higher elongation ratio, with medium value about 12 to 13 for G12 and G14 flax shiv. Wheat straw show the highest elongation ratio with medium value up to 17.8 for G14.

Corn cob are wide and short particles. They are among the widest ones with medium width w_{50} of 3.784 mm and w_{90} of 4.765 mm. Corn cob are the shorter particles with l_{90} equal to 6.472 mm. Their elongation is about 1.5 with a medium elongation ratio of 1.357 ($\varepsilon_{10}=1.142$ and $\varepsilon_{90}= 1.756$).

The results obtained by mechanical sieving are closer to the results obtained by image analysis for width than to the results obtained for length. Actually, as explained in literature for hemp (Amziane and Collet, 2017), the vibration during mechanical sieving, induces the particles to pass through the sieves in a direction perpendicular to the meshes. So, the mechanical sieving results are mainly induced by the width of particles. Moreover, when the particles pass lengthways through the sieves, their width may be oriented along the diagonals d of the square holes and the size to be considered should be $\sqrt{2}.d$ (Igathinathane et al., 2009; Picandet et al., 2012). Such consideration leads to high agreement between mechanical sieving and image analysis for hemp shiv and rape straw. Besides, the image analysis is based on the assumption that the particles shape is quasi-homothetic. The measurement of thickness shows that this is not the case for flax and wheat. For flax, for low values of width, the thickness is nearly constant. Then, the thickness increases with width (Figure 23). For wheat, the thickness is nearly constant, it increases step by step (from grid size to grid size) (Figure 24). Taking this into account allows mechanical sieving curve meeting image analysis curve for width, particularly for the point 1 mm. For wheat, it seems that the discrepancy does not only come from that point. Wheat straw being flexible, maybe it is distorted during the sieving, allowing bigger particles to cross through smaller mesh size.

The particle size distribution of hemp fines and flax fines are close as well with mechanical sieving as with laser diffraction particle sizing. The mechanical sieving leads to lower values than laser diffraction particle sizing. Actually, laser diffraction particle sizing leads to the radius of the equivalent sphere while mechanical sieving leads to the width of particle. This is consistent to find radius value higher than width value. The medium radius is 0.50 mm for hemp fine and 0.56 mm for flax fines.

The dust content ranges from 0.00 % for corn cob to 1.17 % for G7 wheat straw. All the shiv meet the requirement of the French national association Construire en Chanvre. This requirement is defined for hemp shiv: the dust content must be lower than 2 %. More, as underlined in

Table 9, the smaller the shiv is, the higher the dust content is.

Finally, on fiber content point of view, only hemp and flax include fibers. Conversely to dust content, the biggest the shiv is, the highest the fiber content is (except for G14 hemp shiv).
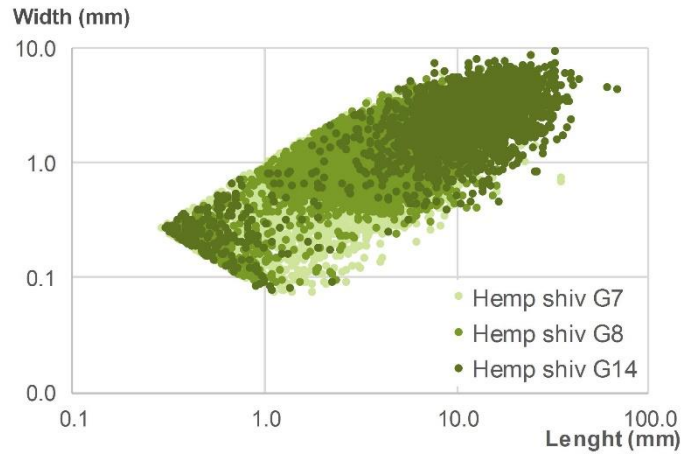
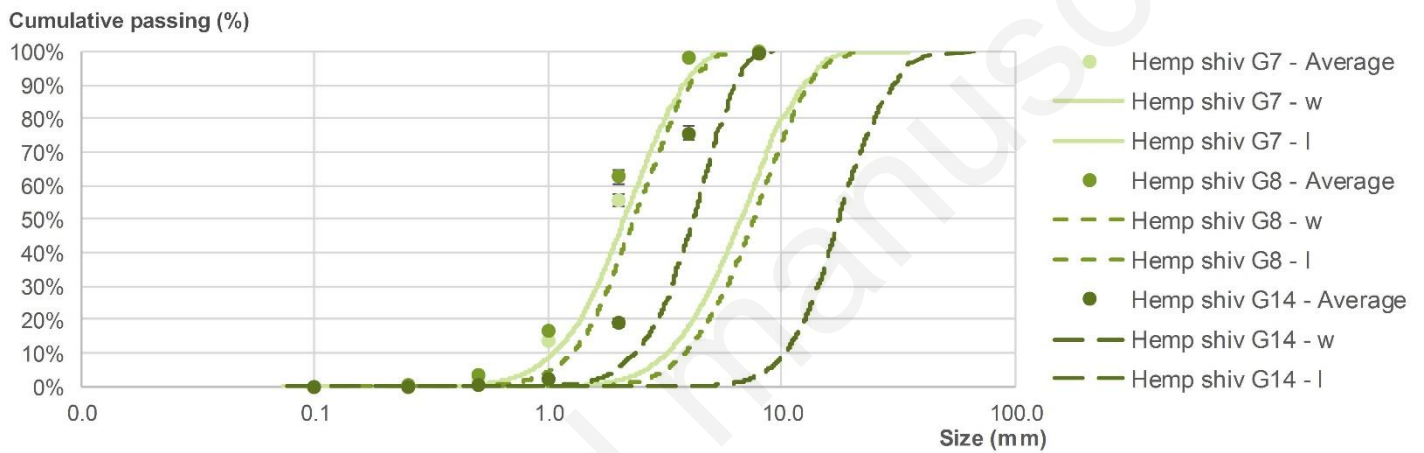*Figure 16: Raw data from image analysis of hemp shiv*

Figure 17: PSD of hemp shiv - mechanical sieving (average and standard deviation) and image analysis (w: width and l: length)
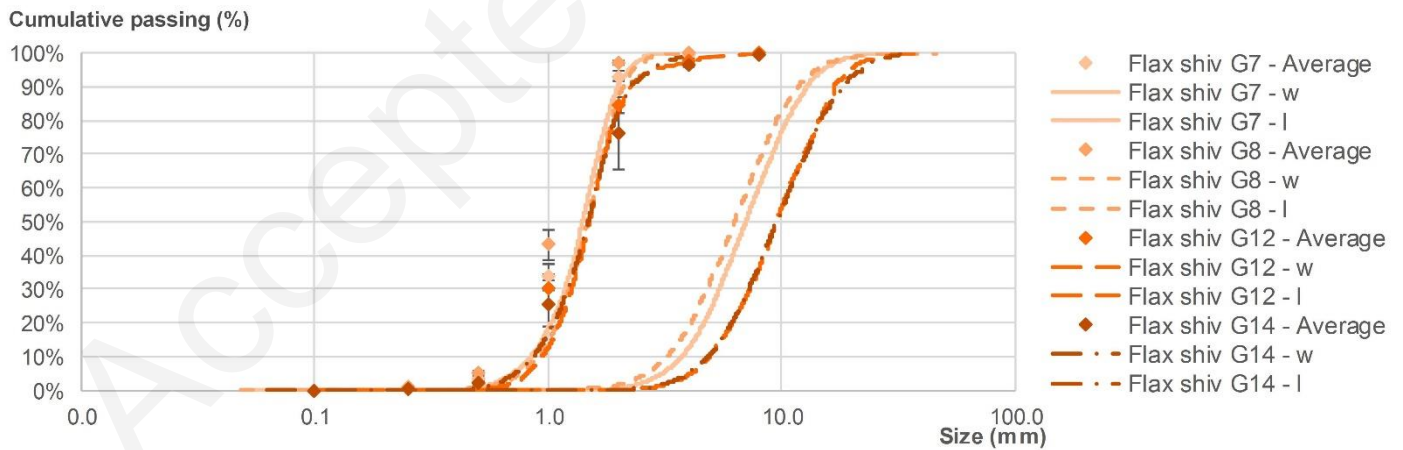

Figure 18: PSD of flax shiv - mechanical sieving (average and standard deviation) and image analysis (w: width and l: length
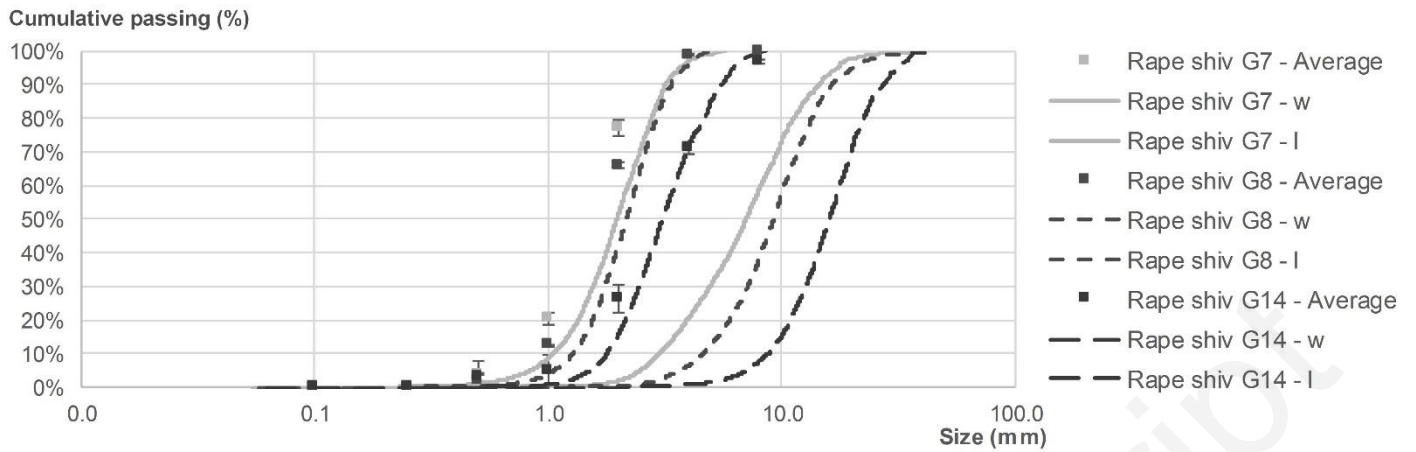
Cumulative passing (%)

Figure 19: PSD of rape straw - mechanical sieving (average and standard deviation) and image analysis (w: width and l: length)

Cumulative passing (%)
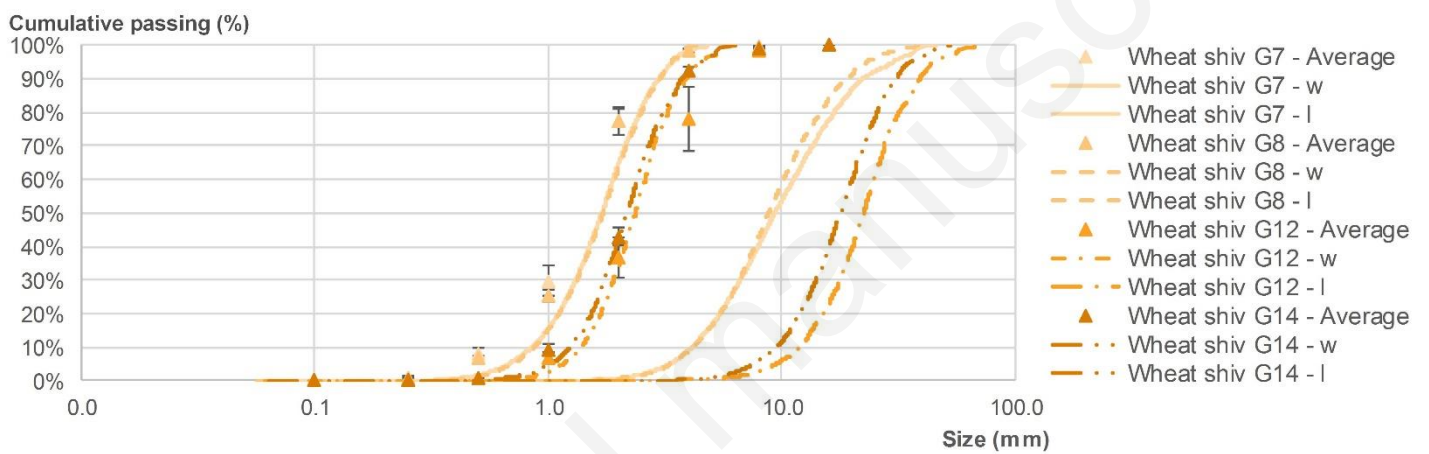

Figure 20: PSD of wheat straw - mechanical sieving (average and standard deviation) and image analysis (w: width and l: length)
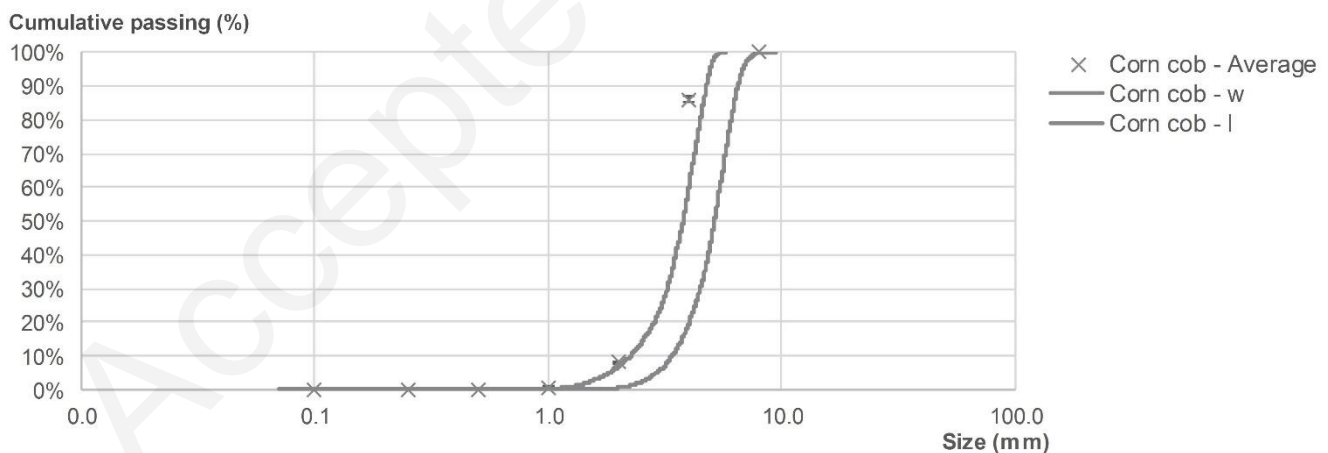
Cumulative passing (%)

Figure 21: PSD of corn cob - mechanical sieving (average and standard deviation) and image analysis (w: width and l: length)
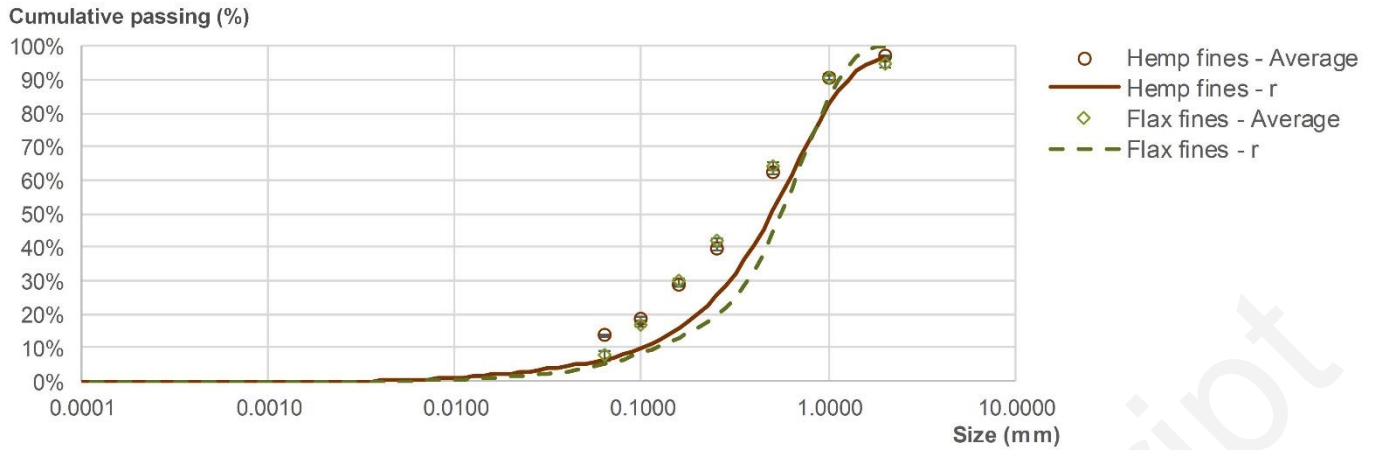
Figure 22: PSD of fines - mechanical sieving (average and standard deviation) and laser diffraction particle sizing (r: radius)

Table 9 : Particle size distributions of hemp shiv, flax shiv, rape straw, wheat straw and corn cob

	Hemp shiv			Flax shiv				Rape straw			Wheat straw				Corn Cob
	G7	G8	G14	G7	G8	G12	G14	G7	G8	G14	G7	G8	G12	G14	
m_{sample} (g)	6.08	6.03	18.04	6.00	6.04	6.00	6.01	6.01	6.03	12.12	6.01	6.00	6.00	6.01	24.03
$n_{particles}$	9274	5513	2267	8327	12909	5460	5827	12321	5853	3303	19512	19923	3615	5151	3753
w_{10} (mm)	1.051	1.257	2.353	0.842	0.898	0.939	0.864	1.050	1.278	1.780	0.848	0.866	1.381	1.239	2.249
w_{50} (mm)	2.105	2.319	4.215	1.402	1.480	1.509	1.485	1.967	2.159	3.079	1.700	1.721	2.360	2.169	3.784
w_{90} (mm)	3.761	4.042	6.275	1.987	2.090	2.257	2.275	3.186	3.389	5.550	2.977	3.005	3.921	3.703	4.765
L_{10} (mm)	3.238	3.859	10.361	3.715	3.242	4.878	4.871	3.005	4.593	8.754	4.112	4.127	11.906	9.463	3.374
L_{50} (mm)	6.703	7.615	17.622	7.014	6.282	9.490	9.509	7.073	9.239	15.922	9.331	8.819	22.466	17.931	5.145
L_{90} (mm)	12.360	13.100	29.993	12.763	11.720	16.753	18.495	14.639	16.362	27.270	22.031	19.106	39.022	30.901	6.472
ε_{10}	1.765	1.849	2.481	2.615	2.291	3.115	3.301	1.509	1.995	2.630	2.488	3.080	4.856	3.872	1.142
ε_{50}	3.052	3.142	4.250	5.204	4.349	6.262	6.582	3.585	4.345	5.105	6.013	6.544	9.482	8.372	1.357
ε_{90}	5.678	5.655	7.921	10.154	8.418	12.270	12.793	7.714	8.936	9.789	12.861	12.920	17.845	15.535	1.756
Dust content	0.80%	0.65%	0.04%	0.46%	0.74%	0.25%	0.21%	0.31%	0.14%	0.02%	1.17%	1.03%	0.05%	0.06%	0.00%
Fibre content	5.01%	6.51%	2.31%	4.64%	1.66%	5.37%	8.09%	0.00%	0.00%	0.00%	0.00%	0.00%	0.00%	0.00%	0.00%

Table 10: Particle size distribution of fines (hemp and flax)

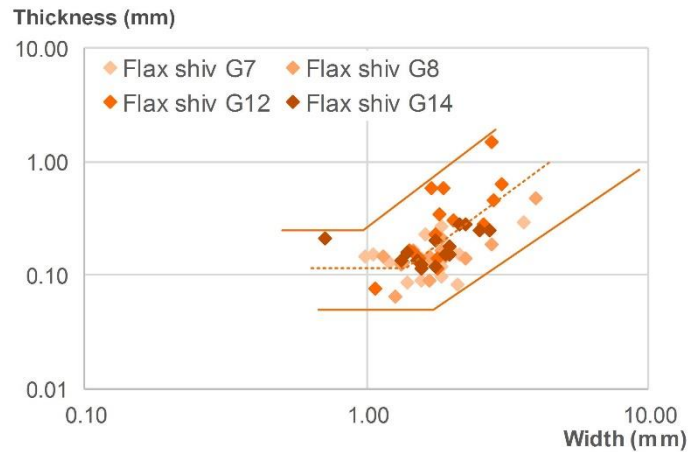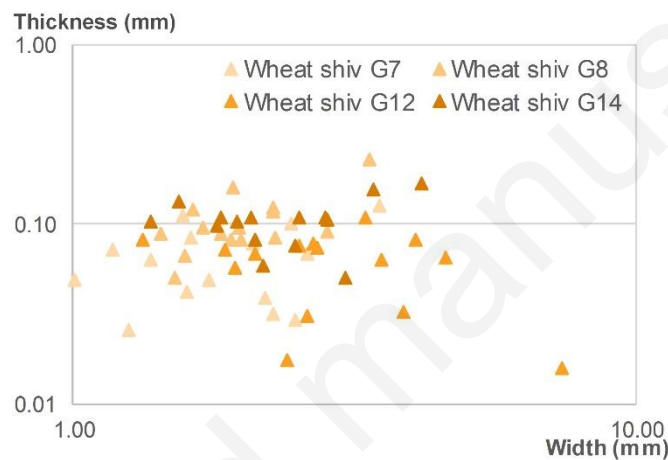|	Hemp fines	Flax fines
$r_{10\ (laser)}$	0.100	0.112
$r_{50\ (laser)}$	0.502	0.564
$r_{90\ (laser)}$	1.262	1.125

Figure 23: Flax - Thickness versus width

Figure 24: Wheat - thickness versus width

Table 11: Particle Size distribution of hemp shiv - bibliography

Aggregate	LCDA Hemp shiv	Hemp shiv	LCDA Hemp shiv 1	LCDA Hemp shiv 2	LCDA Hemp shiv 3	"Chanvre d'Auvergne" Hemp Shiv
Reference	(Nguyen et al., 2009)	(Chabannes et al., 2014)	(Arnaud and Gourlay, 2012)			(Nozahic et al., 2012)
w_{10} (mm)	0.7	1.55				0.85
w_{50} (mm)	2	2.7	2	1.8	1	1.75
w_{90} (mm)	4.2	4				3.1
L_{10} (mm)	3.7	5				3.5
L_{50} (mm)	9	9.5	8.9	7.6	3.1	7
L_{90} (mm)	18	17.5				14

3.3.2. Density and porosity

The bulk density, skeleton density and open porosity are given in Table 12 and Figure 25. The standard deviation between the five measurements of bulk density is very low for all agro-resources. This leads to a coefficient of variation lower than 5 %, showing the accuracy of measurement. All aggregates are characterized by a low density and a high porosity.

Overall, the bulk density of aggregates decreases when the size of aggregates increases. For hemp shiv, the bulk density at dry state ranges from 88 to 104 kg/m³. Flax shiv show slightly higher values from 91 to 130 kg/m³. Rape straw and wheat straw show lower values, from 73 to 88 kg/m³ and from 29 to 54 kg/m³ respectively. Fines show higher density than shiv (133 kg/m³ for hemp and 140 kg/m³ for flax). Finally, corn cob has the highest bulk density (373 kg/m³).

These values are in the range commonly met in literature (Table 13), except for rape straw for which they are one third less. This may be due to the shiv size. The bulk density of G7 hemp shiv is very close to the values found in (Nozahic et al., 2012), (Arnaud and Gourlay, 2012) and (Nguyen et al., 2009). The bulk density of G7 and G8 flax shiv are close to the values given in (Chabriac et al., 2016) while the bulk density of G12 and G14 flax shiv meet the values of (Rahim et al., 2016a). For wheat straw, the bulk density of G12 and G14 are close to the values given in (Bouasker et al., 2014).

For a given agro-resource, the skeleton density is similar for all sizes of shiv. The skeleton densities of corn cob, flax shiv and hemp shiv are close (with average values of 1333, 1342 and 1352 kg/m³ respectively). The skeleton densities of rape straw and wheat straw are 5 to 10 % higher (1411 and 1478 kg/m³). The skeleton density of fines (1557 kg/m³ for hemp and 1458 kg/m³ for flax) is higher than the skeleton density of shiv. This is due to the fact that fines include fibers and that the density of fibers is higher than the density of shiv. These results meet the values found in bibliography for hemp and flax. For hemp, the skeleton density ranges from 1257 kg/m³ for G14 hemp shiv to 1401 kg/m³ for G7 hemp shiv while the values given in (Rahim et al., 2016a) and in (Nguyen et al., 2009) are respectively 1259 and 1465 kg/m³, respectively. For flax, the skeleton density is 5 % higher than the value given in (Rahim et al., 2016b) and more scattered with the value in (Chabriac et al., 2016) (by 16 %). For rape, the skeleton density given in (Rahim et al., 2016a) is 17.6 % lower than the value found here. For wheat straw, there is much more discrepancy, as Bouasker et al. (Bouasker et al., 2014) found skeleton density ranging from 865 to 871 kg/m³.

The open porosity, including inter-particles and intra-particles porosity, is high. For corn cob, it is equal to 72 %. For all other aggregates, it is higher than 90 %: (i) 90-91 % for fines, (ii) about 92 to 94 % for hemp shiv, flax shiv and rape straw, (iii) up to 96-98 % for wheat straw. A slight increase of porosity with aggregate size can be noticed. Once again, the results meet the values found in bibliography. For hemp shiv, the porosity is in agreement with values found in (Nguyen et al., 2009) and (Rahim et al., 2016a). There is a slight discrepancy with values found in (Chabriac et al., 2016) (6.3 %). For flax, the value meets the values given in (Chabriac et al., 2016) and (Rahim et al., 2016a), with discrepancy lower than 2 %. For wheat straw, the porosity meets the value given in (Bouasker et al., 2014) where it is 96 to 97 %.

Finally, Figure 26 shows the relationship between open porosity, bulk density and skeleton density of agro-resources. The open porosity evolves in a plan with the (bulk density; skeleton density) pair.

Table 12 : Bulk density at dry state, skeleton density and open porosity of agro-aggregate

|		Hemp shiv				Flax shiv					Rape straw			Wheat straw				Corn Cob
		G7	G8	G14	fines	G7	G8	G12	G14	fines	G7	G8	G14	G7	G8	G12	G14	Corn Cob
Bulk density at dry state (kg/m³)	Av.	104.01	87.89	96.65	133.21	111.28	129.91	93.69	90.72	140.30	88.06	78.71	73.20	53.89	49.70	29.69	31.20	372.75
	σ	1.44	0.62	2.70	4.24	3.49	3.05	1.48	1.61	3.26	1.05	2.13	0.93	0.51	2.35	1.20	1.18	3.66
	CoV	1.38%	0.71%	2.79%	3.19%	3.14%	2.35%	1.58%	1.77%	2.32%	1.19%	2.71%	1.28%	0.95%	4.73%	4.04%	3.79%	0.98%
Skeleton density (kg/m³)		1401	1399	1257	1557	1367	1321	1344	1335	1458	1430	1385	1418	1486	1408	1483	1534	1333
Skeleton density (kg/m³)	Av.	1352			1557	1342				1458	1411			1478				1333
	σ	83			-	19				-	23			52				-
	CoV	6.11%			-	1.44%				-	1.64%			3.53%				-
Open porosity (%)		92.58%	93.72%	92.31%	91.45%	91.86%	90.17%	93.03%	93.20%	90.37%	93.84%	94.32%	94.84%	96.37%	96.47%	98.00%	97.97%	72.05%
Open porosity (%)	Av.	92.87%			91.45%	92.06%				90.37%	94.33%			97.20%				72.05%
	σ	0.75%			-	1.40%				-	0.50%			0.90%				-
	CoV	0.80%			-	1.52%				-	0.53%			0.93%				-
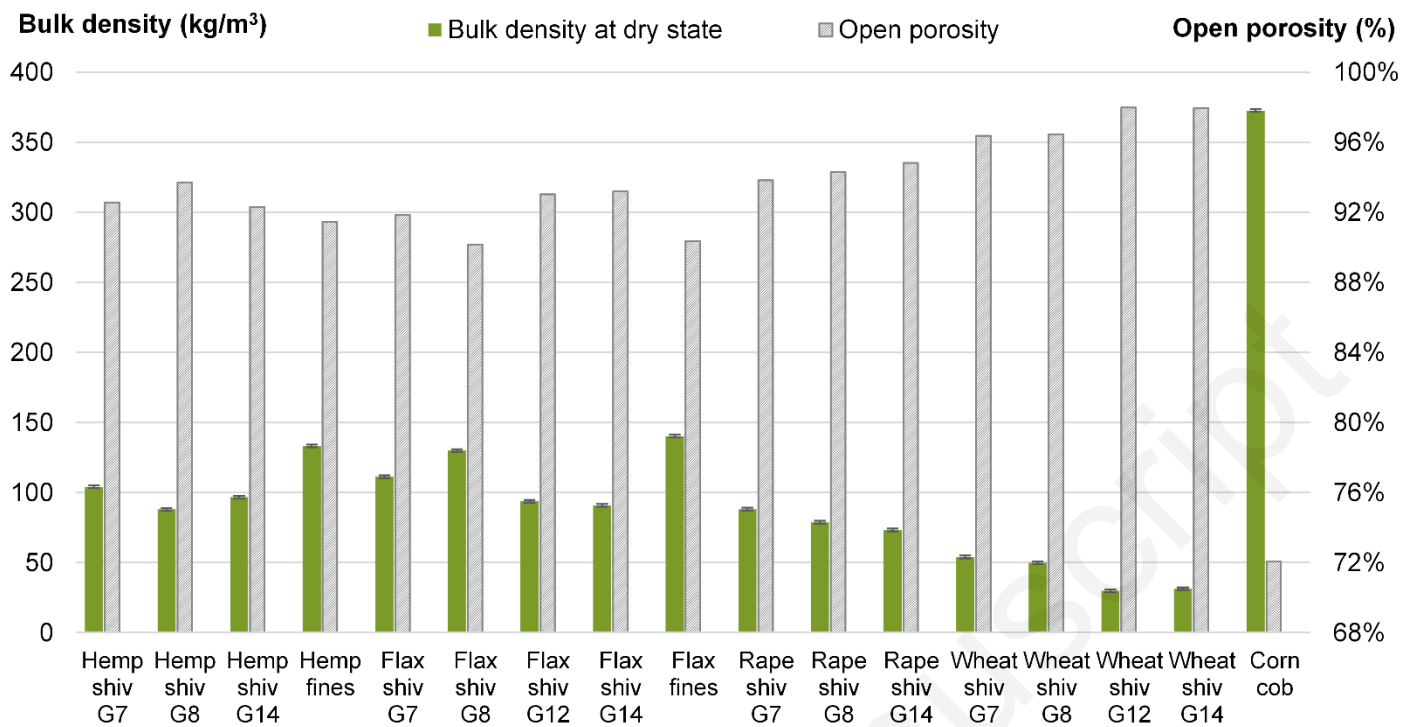
Figure 25: Bulk density at dry state and open porosity of agro-aggregate

Table 13: Bulk density, skeleton density and porosity of agro-aggregates from literature

Aggregate	Bulk density (kg/m³)	Skeleton density (kg/m³)	Total Porosity (%)	Reference
LCDA hemp shiv	103	1465	92.9	(Nguyen, 2010)
Terrachanvre fibered hemp shiv	54.8	1438	96.2	
Chanvre d'Auvergne hemp shiv	103	-	-	(Nozahic et al., 2012)
Hemp Shiv	103.5 ± 4	-	-	(Chabannes et al., 2014)
Hemp shiv	133	1020	87	(Chabriac et al., 2016)
Flax shiv	115	1120	90.5	
Rape straw	115	1150	90	
Hemp shiv	125	1259	90.01	(Rahim et al., 2016a)
Flax shiv	90	1270	92.9	
Rape straw	130	1162	88.8	
Wheat straw fiber	25-33	865-871	96-97	(Bouasker et al., 2014)
LCDA Hemp shiv 1	112	-	-	(Arnaud and Gourlay, 2012)
LCDA Hemp shiv 2	114	-	-	
LCDA Hemp shiv 3	119	-	-	

$$n_O = -0.0736\rho_b + 0.0046\rho_s + 93.6925$$
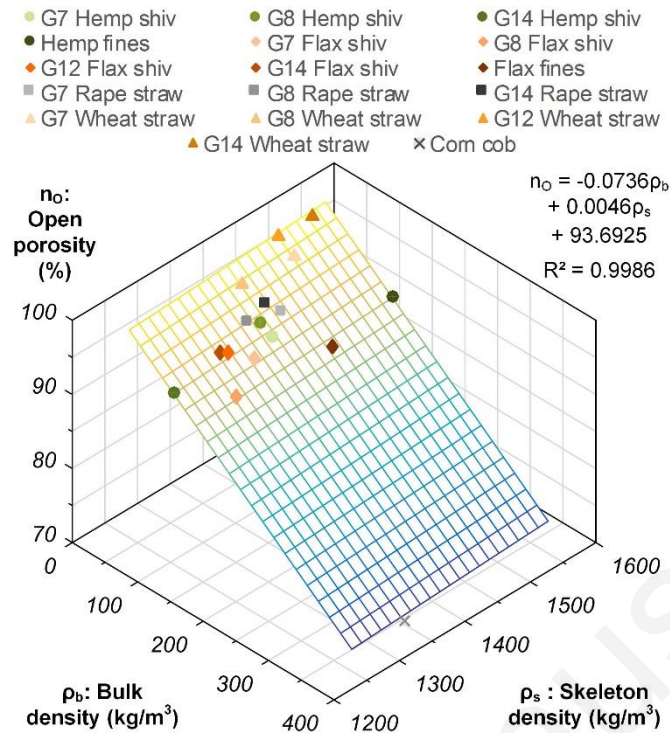$$R^2 = 0.9986$$

Figure 26: Open porosity versus bulk density and skeleton density of agro-resources

3.3.3. Water absorption

Figure 27 gives the example of G7 wheat straw for the investigation of water absorption. It shows the experimental data of the three samples, their fitting curves and the characteristic curve obtained by averaging the fitting curve coefficients of the three samples. For all aggregates, Table 14 gives the average values and standard deviations of fitting curve coefficient (IRA and K1) and correlation coefficients.

For all shiv and straw, the coefficients of variation of IRA and of K1 are lower than 10 % (even lower than 5 %) and the correlation coefficient is very high (>0.93, except for one sample of G12 wheat straw). This induces a high confidence in the results. For corn cob, the coefficients of variation are slightly higher (11.6 % for IRA and 15.2 % for K1) but the correlation coefficients are high too (0.96). There is slightly more discrepancy between the results of corn cob. For fines, the coefficient of variation are high (for hemp: about 20 % for IRA and for K1, for flax: about 40 % for IRA but only 2.4 % for K1). The correlation coefficients are lower than for shiv (0.81 for hemp and 0.89 for flax). As a matter of fact, during the measurement some fines pass through the permeable bag as they are smaller than the mesh. This partially distorts the results, particularly for long time measurements. The results are thus much less accurate for fines than for shiv.

For a given raw material, the initial rate of absorption IRA and the slope of the curve K1 are close for all sizes of shiv. As shown in Table 14 and on Figure 28 to Figure 33, the IRA is the lowest for flax shiv with values about 130 %, it is the highest for rape straw with values higher than 200 % and up to 250 %. The IRA of hemp shiv and wheat straw are close, about 190 % (except for G14 hemp shiv for which it is 140 % only). The K1 slope is the lowest for flax shiv and wheat straw with values about 40 %.log(min)$^{-1}$. For rape straw, K1 ranges from 40 to 52 %.log(min)$^{-1}$. The highest slope is the slope of hemp shiv, with values from 52 to 58 %.log(min)$^{-1}$. Finally, the water content at 48 hours are the lowest for flax shiv (from 250 to 300 %), the highest for rape straw (from 386 to 394 %). The water content at 48 hours of hemp shiv and of wheat straw range respectively from 340 to 380 % and from 308 to 345 %, respectively.

Fines show a significantly different behavior. For hemp, the IRA of fines is about 280 %: it is much higher than the IRA of shiv. Conversely, for flax the IRA of fines is about 35 %, this is much lower than the IRA of shiv. For both types of fines, the slope is much higher: about 74 %.log(min)$^{-1}$ for hemp and 88 %.log(min)$^{-1}$ for flax. After 48 hours of absorption, the water content of flax fine is about 340 %. It is higher than the values obtained with flax shiv despite the IRA is lower for fine than for shiv. The water content of hemp fine at 48 hours is 540 %, much higher than the highest value found for all shiv.

Whatever the time of absorption, corn cob shows substantially smaller water content than all kinds of shiv. Its IRA is about 72 % and its K1 slope is 32 %.log(min)$^{-1}$, leading to a water content at 48 hours of 182 %.

The water absorptions found for hemp shiv are in the range of values found in bibliography (Figure 29, Figure 32 and Table 15). For G14 hemp shiv, the results are very close to those found in (Chabannes et al., 2014; Magniont et al., 2012).
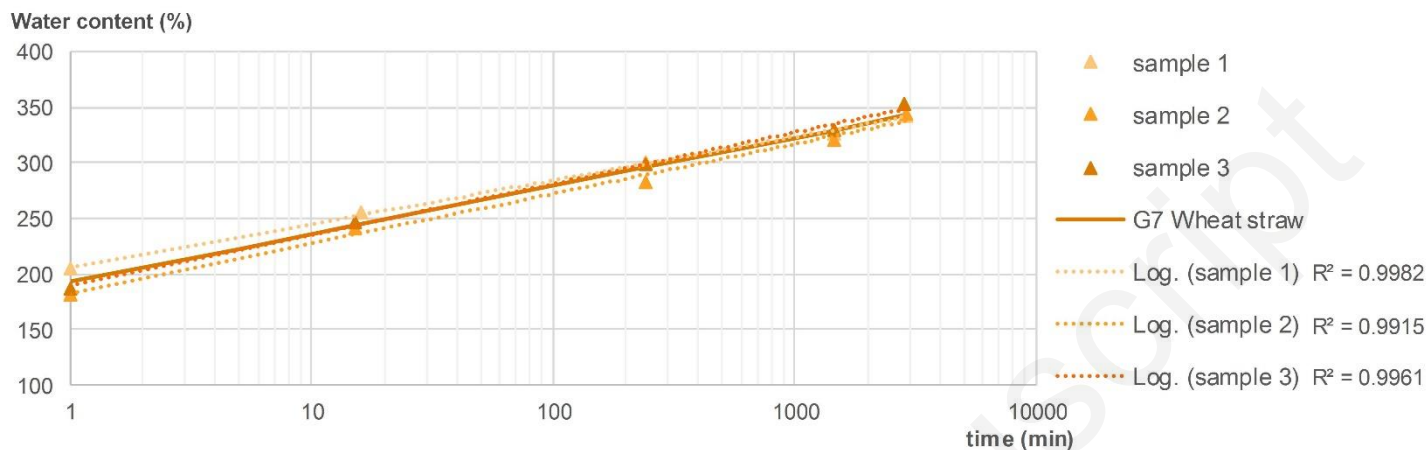

Figure 27: water absorption of G7 wheat straw - experimental data, fitting curves and characteristic curve of G7 wheat straw

Table 14: Characteristic curves of water absorption versus logarithmic time – average values and standard deviations of fitting curve parameters and correlation coefficients

| | | Hemp shiv | | | | Flax shiv | | | | | Rape straw | | | Wheat straw | | | | Corn Cob |
		G7	G8	G14	fines	G7	G8	G12	G14	fines	G7	G8	G14	G7	G8	G12	G14	
IRA	Av.	191.05	192.90	140.51	283.82	122.07	162.37	126.27	124.55	34.72	221.68	253.26	206.12	192.61	206.86	185.31	174.55	71.70
	σ	7.76	4.54	6.92	51.66	5.61	6.34	6.90	10.04	14.69	4.39	5.04	3.62	12.15	4.79	3.00	7.82	8.33
	CoV	4.06%	2.35%	4.93%	18.20%	4.60%	3.90%	5.46%	8.06%	42.30%	1.98%	1.99%	1.75%	6.31%	2.32%	1.62%	4.48%	11.61%
K1	Av.	54.25	52.12	57.82	74.35	41.43	39.79	36.88	37.70	87.81	48.99	40.60	52.16	43.25	40.02	42.66	38.71	31.84
	σ	2.68	3.25	2.06	16.43	3.93	2.30	0.81	2.92	2.08	2.06	2.65	0.74	3.79	5.94	0.66	3.03	4.85
	CoV	4.93%	6.25%	3.56%	22.10%	9.48%	5.78%	2.19%	7.74%	2.36%	4.20%	6.52%	1.41%	8.77%	14.85%	1.54%	7.82%	15.23%
r²	Av.	0.952	0.959	0.957	0.808	0.938	0.977	0.977	0.940	0.887	0.963	0.954	0.981	0.995	0.966	0.917	0.994	0.961
	σ	0.014	0.031	0.016	0.044	0.038	0.010	0.012	0.033	0.053	0.005	0.056	0.013	0.003	0.027	0.032	0.005	0.013
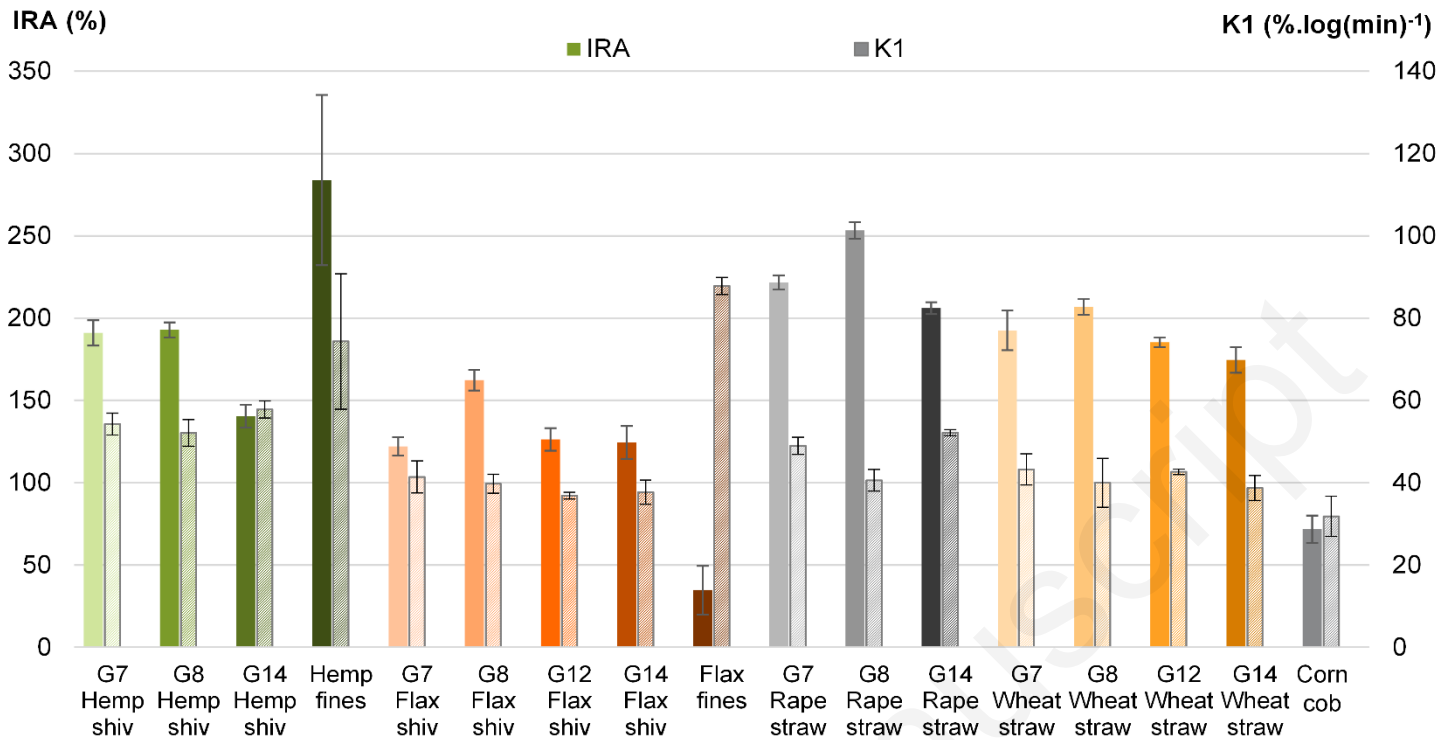
Figure 28: Water absorption, average values and standard deviations of fitting curve parameters IRA and K1
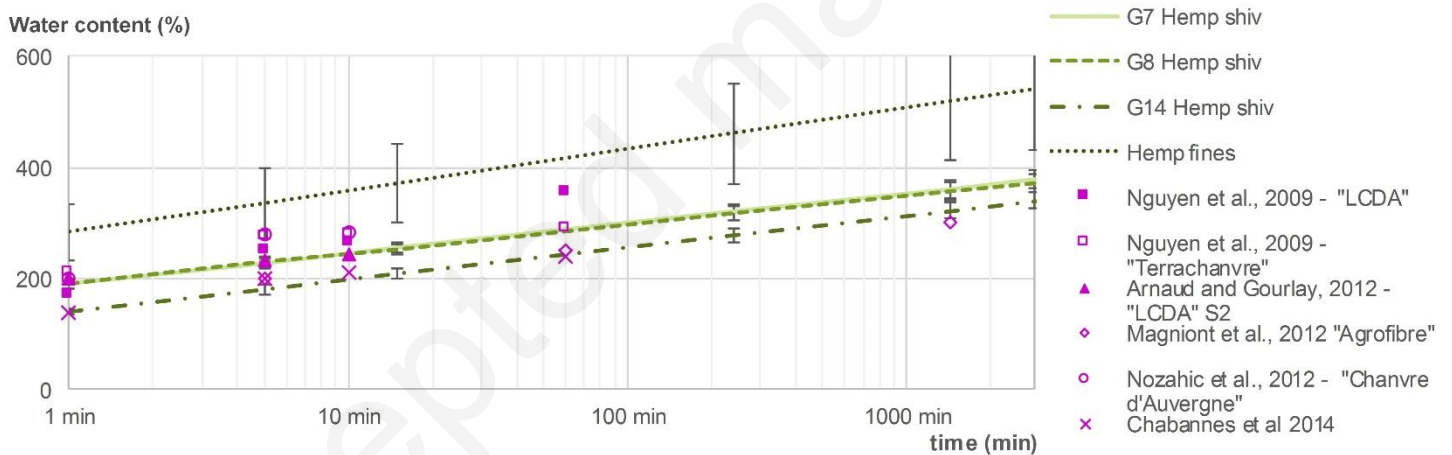

Figure 29: Water absorption of hemp shiv and fines compared with (Arnaud and Gourlay, 2012; Chabannes et al., 2014; Magniont et al., 2012; Nguyen et al., 2009; Nozahic et al., 2012)
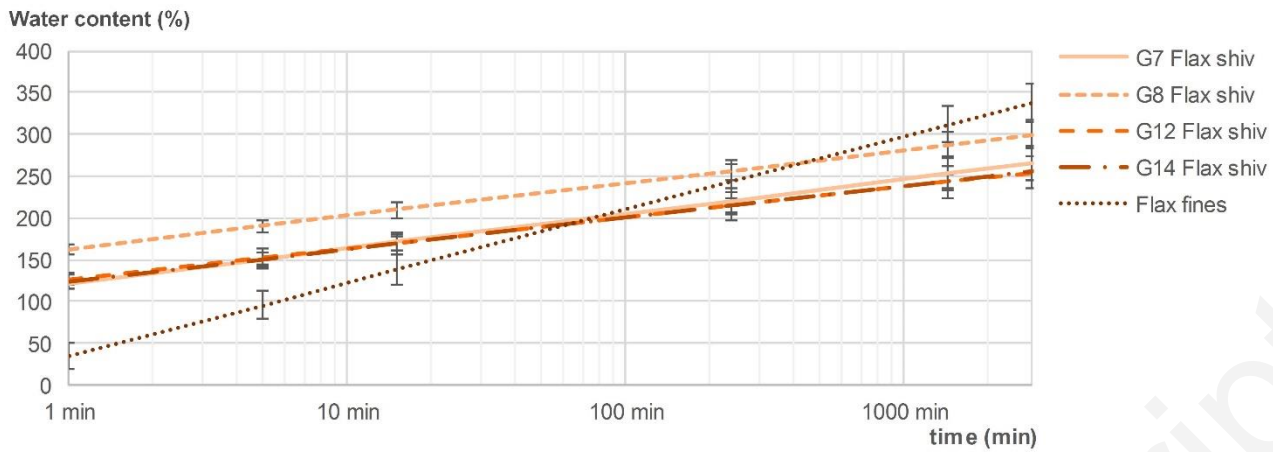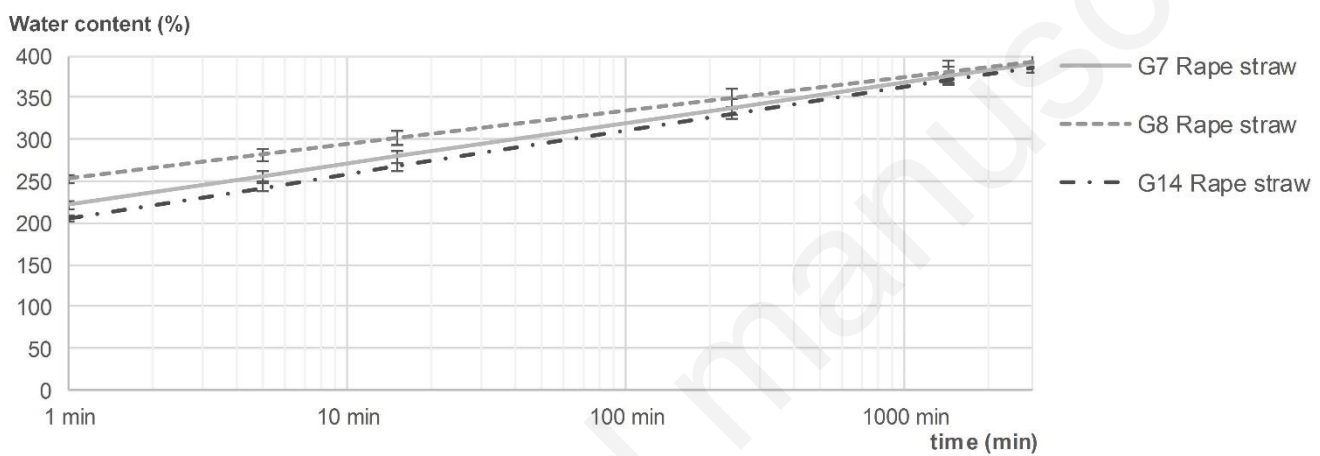
Figure 30: Water absorption of flax shiv and fines

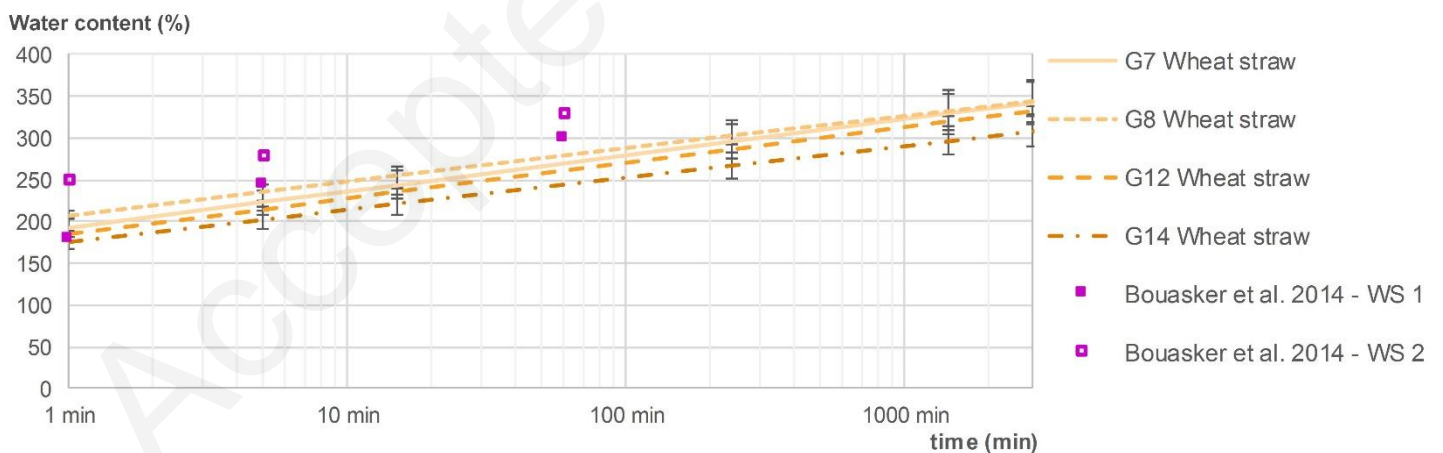*Figure 31: Water absorption of rape straw*

Figure 32: Water absorption of wheat straw compared with (Bouasker et al., 2014)
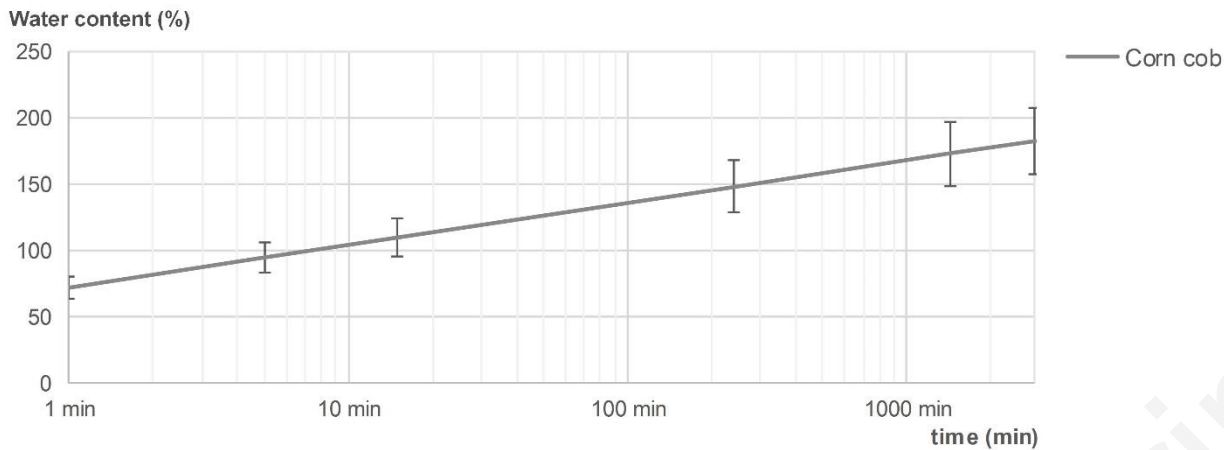
Figure 33: Water absorption of corn cob

Table 15: Water absorption of agro-aggregates from literature

| Aggregate | Water absorption versus time (%) | | | | | Reference |
	1 min.	5 min.	10 min.	60 min.	1440 min.	
"Terrachanvre" fibered hemp shiv	170 %	250 %	265 %	356 %	-	(Nguyen et al., 2009)
"LCDA" Hemp Shiv	210 %	275 %	280 %	290 %	-	(Nguyen et al., 2009)
"LCDA - HS 2" Hemp Shiv	200 %	232 %	242 %	-	-	(Arnaud and Gourlay, 2012)
"Agrofibre" Hemp Shiv	-	200 %	-	250 %	300 %	(Magniont et al., 2012)
"Chanvre d'Auvergne" Hemp Shiv	200 %	280 %	285 %	-	-	(Nozahic et al., 2012)
Hemp Shiv	138 %	200 %	210 %	240 %	-	(Chabannes et al., 2014)
Wheat straw S1	180 %	245 %	-	300 %	-	(Bouasker et al., 2014)
Wheat straw S2	250 %	280 %	-	330 %	-	(Bouasker et al., 2014)

3.3.4. Thermal conductivity

Table 16 and Figure 34 summarize the thermal conductivity versus bulk density at (23°C, dry state) of all aggregates. For each aggregate, the coefficient of variation is lower than 5% as well for bulk density as for thermal conductivity. This induces high confidence in the results. The thermal conductivity ranges from 0.045 to 0.093 W/(m.K) for bulk density ranging from 30 to 392 kg/m^3. Globally, the thermal conductivity increases linearly with bulk density. Corn cob shows much higher thermal conductivity than other aggregates due to much higher bulk density. Indeed, the thermal conductivity of corn cob is 0.093 W/(m.K) when it ranges from 0.045 to 0.058 W/(m.K) for other aggregates. For a given raw material, the discrepancy between thermal conductivity of shiv obtained with several grid size is low (coefficient of variation lower than 4 % whatever the raw material) even if the discrepancy between bulk density is high (up to 30%). Thus, the thermal conductivity depends on raw material too. Wheat straw shows the lowest thermal conductivity, about 0.045 W/(m.K). Rape straw shows slightly higher values than wheat straw, about 0.05 W/(m.K). Flax shiv and hemp shiv show similar values of thermal conductivity, about 0.54 W/(m.K). Finally, the thermal conductivity of fines is higher than the thermal conductivity of shiv (0.058 W/(m.K) for flax fines). Regarding the standard NF P75-101 (AFNOR, 1983), all aggregates are thermal insulators (λ < 0.065 W/(m.K)), except corn cob.

Table 16: Thermal conductivity versus bulk density at (23°C; dry state)

		Hemp shiv				Flax shiv					Rape straw			Wheat straw				Corn Cob
		G7	G8	G14	fines	G7	G8	G12	G14	fines	G7	G8	G14	G7	G8	G12	G14	
Bulk density (kg/m³)	Av.	104.01	87.89	97.36	133.21	111.23	129.91	93.69	90.72	140.30	88.26	78.71	73.26	53.92	49.70	29.69	31.23	392.44
	σ	0.05	0.62	0.44	4.24	0.04	3.05	1.48	0.06	3.26	0.30	2.13	0.11	0.36	2.35	1.20	0.07	2.38
	CoV	0.04%	0.71%	0.45%	3.19%	0.03%	2.35%	1.58%	0.06%	2.32%	0.34%	2.71%	0.15%	0.66%	4.73%	4.04%	0.24%	0.61%
Bulk density (kg/m³)	Av.	96.42			133.21	106.39				140.30	80.08			41.13				392.44
	σ	8.10			-	18.11				-	7.59			1.02				-
	CoV	8.40%			-	17.02%				-	9.48%			2.49%				-
Thermal conductivity (W/(m.K))	Av.	0.0543	0.0530	0.0532	0.0543	0.0540	0.0577	0.0534	0.0531	0.0575	0.0499	0.0497	0.0499	0.0457	0.0457	0.0446	0.0451	0.0926
	σ	0.0008	0.0011	0.0008	0.0010	0.0013	0.0013	0.0022	0.0006	0.0011	0.0006	0.0006	0.0014	0.0009	0.0003	0.0005	0.0002	0.0017
	CoV	1.55%	2.11%	1.42%	1.82%	2.48%	2.33%	4.19%	1.11%	2.00%	1.26%	1.24%	2.75%	2.07%	0.68%	1.20%	0.46%	1.86%
Thermal conductivity (W/(m.K))	Av.	0.0535			0.0543	0.0546				0.0575	0.0498			0.0453				0.0926
	σ	0.0007			-	0.0022				-	0.0001			0.0003				-
	CoV	1.36%			-	3.95%				-	0.29%			0.72%				-

Thermal conductivity λ (W/(m.K))

$$\lambda = 0.0001\rho + 0.0398$$
$$R^2 = 0.9866$$

- Hemp shiv G7
- Hemp shiv G8
- Hemp shiv G14
- Hemp fines
- Flax shiv G7
- Flax shiv G8
- Flax shiv G12
- Flax shiv G14
- Flax fines
- Rape straw G7
- Rape straw G8
- Rape straw G14
- Wheat straw G7
- Wheat straw G8
- Wheat straw G12
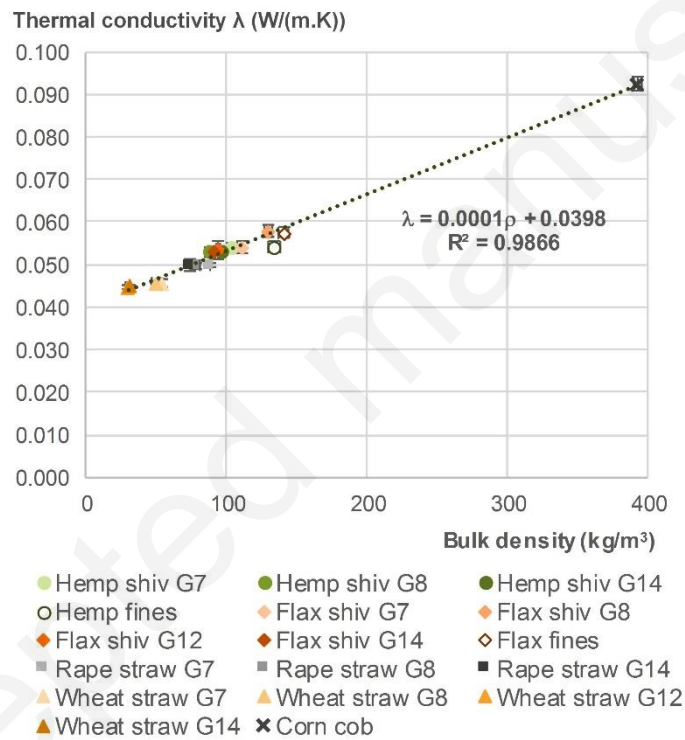- Wheat straw G14
- Corn cob

Figure 34: Thermal conductivity versus bulk density at (23°C, dry state)

Table 17 summarizes thermal conductivity of agro-aggregates found in literature. The thermal conductivities of hemp shiv are in the range of bibliography. They are about 5 % higher than values found in (Rahim et al., 2016a) and 2 % lower than values given in (Balčiūnas et al., 2016). For rape straw, the values of thermal conductivity are close to the values found in literature too. They are about 5 % higher than the value given in (Rahim et al., 2016a). For flax shiv, there is more discrepancy with bibliography. Actually, the thermal conductivity of flax shiv given in (Rahim et al., 2016a) is 22 % lower than the value found here. However, in (Rahim et al., 2016a), a self-consistent scheme is used to model the thermal conductivity of bio-based concrete. Experimental data and modelling are in good agreement for hemp concrete and flax concrete and are more scattered for flax concrete. According to the authors, this can be explained by the simplified description of the geometrical model. This may also come from the value of thermal conductivity of flax shiv which can be underestimated.

Wheat straw is the best thermal insulator. Hemp, flax and rape are also good thermal insulators.

Table 17: Thermal conductivity of agro-aggregates from literature

Aggregate	Conditioning	Bulk density (kg/m³)	Thermal conductivity (W/(m.K))	Reference
Hemp shiv	-	110	0.048	(Cerezo, 2005)
Hemp shiv	-	155	0.058	(Cerezo, 2005)
0/2.5 Hemp shiv	dry state	-	0.055	(Balčiūnas et al., 2016)
2.5/5 Hemp shiv	dry state	-	0.053	(Balčiūnas et al., 2016)
5/10 Hemp shiv	dry state	-	0.055	(Balčiūnas et al., 2016)
10/20 Hemp shiv	dry state	-	0.059	(Balčiūnas et al., 2016)
0/20 Hemp shiv	dry state	-	0.054	(Balčiūnas et al., 2016)
Hemp shiv	20°C, dry state	-	0.050	(Rahim et al., 2016a)
Hemp shiv	30°C, dry state	-	0.052	(Rahim et al., 2016a)
Flax shiv	20°C, dry state	-	0.042	(Rahim et al., 2016a)
Flax shiv	30°C, dry state	-	0.044	(Rahim et al., 2016a)
Rape straw	20°C, dry state	-	0.047	(Rahim et al., 2016a)
Rape straw	30°C, dry state	-	0.049	(Rahim et al., 2016a)

3.3.5. Moisture Buffer Value

Table 18 and Figure 35 give the moisture buffer value for each type of aggregates. Figure 36 gives a synthesis of moisture buffer value versus bulk density. Considering all agro-resources, the MBV increases with bulk density. Table 18 also gives the average MBV of a given agro resource (from the results obtained on different grid sizes). For a given agro-resource, the results obtained with the different grid sizes are close, the coefficient of variation is low.

Wheat straw has the smallest MBV, ranging from 1.88 to 1.97 g/(m².%RH). According the Nordtest project classification (Rode et al., 2005), it is a good hygric regulator (MBV between 1 and 2 g/(m².%RH)).

Hemp shiv, rape straw and flax shiv show similar MBV ranging from 2.07 to 2.36 g/(m².%RH), with average values about 2.21 to 2.26 g/(m².%RH). According the Nordtest project classification, they are excellent hygric regulators (MBV higher than 2 g/(m².%RH)).

Corn cob shows the highest performances with MBV of 3.11 g/(m².%RH).

All these aggregates are very interesting on moisture buffering capacity point of view.

Table 18: Moisture Buffer Value in adsorption, desorption and average - average value, standard deviation and coefficient of variation between the three samples of a given aggregate and average value, standard deviation and coefficient of variation between grid sizes of given agro resource.

|		Hemp shiv				Flax shiv					Rape straw			Wheat straw				Corn Cob
		G7	G8	G14	fines	G7	G8	G12	G14	fines	G7	G8	G14	G7	G8	G12	G14	
Bulk density after stabilization at 23°C and 50%RH (kg/m³)	Av.	118.23	101.03	112.80	151.19	121.07	140.49	111.33	109.37	157.80	109.54	84.75	90.95	68.44	58.94	37.37	38.36	405.68
	σ	2.39	0.00	2.11	0.00	3.69	0.00	0.00	1.46	0.00	1.66	0.00	1.01	8.14	0.00	0.00	0.54	6.39
	CoV	2.03%	0.00%	1.87%	0.00%	3.05%	0.00%	0.00%	1.33%	0.00%	1.52%	0.00%	1.11%	11.89%	0.00%	0.01%	1.41%	1.58%
MBV Ads. (g/(m².%RH))	Av.	2.26	2.02	2.26	2.23	2.25	2.12	2.15	2.36	2.46	2.21	2.16	2.23	1.88	1.95	1.87	1.95	2.98
	σ	0.04	0.03	0.09	0.07	0.08	0.04	0.07	0.23	0.05	0.06	0.03	0.06	0.03	0.02	0.07	0.18	0.16
	CoV	1.90%	1.45%	3.76%	3.13%	3.37%	1.72%	3.29%	9.85%	1.92%	2.59%	1.29%	2.75%	1.62%	1.00%	3.90%	9.39%	5.36%
MBV Des. (g/(m².%RH))	Av.	2.32	2.12	2.28	2.32	2.30	2.31	2.28	2.36	2.55	2.24	2.26	2.26	1.89	1.99	1.88	1.92	3.23
	σ	0.04	0.03	0.09	0.06	0.08	0.04	0.06	0.22	0.05	0.06	0.02	0.05	0.03	0.02	0.06	0.19	0.15
	CoV	1.89%	1.57%	3.89%	2.73%	3.36%	1.59%	2.61%	9.46%	1.86%	2.61%	0.88%	2.22%	1.77%	1.14%	3.31%	9.66%	4.63%
MBV Av. (g/(m².%RH))	Av.	2.29	2.07	2.27	2.27	2.27	2.21	2.21	2.36	2.50	2.22	2.21	2.25	1.88	1.97	1.88	1.94	3.11
	σ	0.04	0.03	0.09	0.07	0.07	0.04	0.07	0.23	0.05	0.06	0.02	0.05	0.03	0.02	0.07	0.18	0.15
	CoV	1.79%	1.51%	3.82%	2.92%	3.25%	1.65%	2.94%	9.58%	1.89%	2.56%	1.02%	2.45%	1.66%	1.03%	3.52%	9.40%	4.93%
MBV Av. agro-resource (g/m².%RH))	Av.	2.21			2.27	2.26				2.50	2.23			1.92				3.11
	σ	0.12			-	0.07				-	0.02			0.07				-
	CoV	5.48%			-	2.98%				-	0.78%			3.86%				-
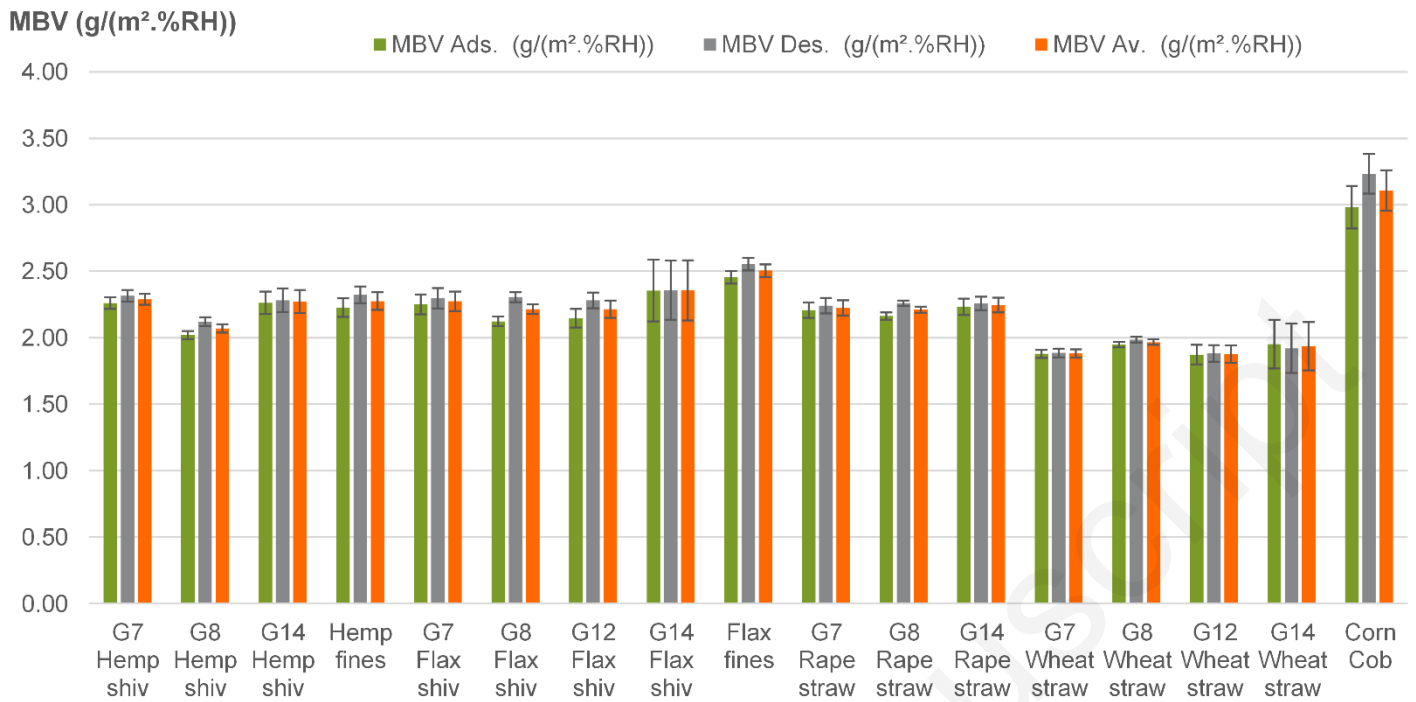
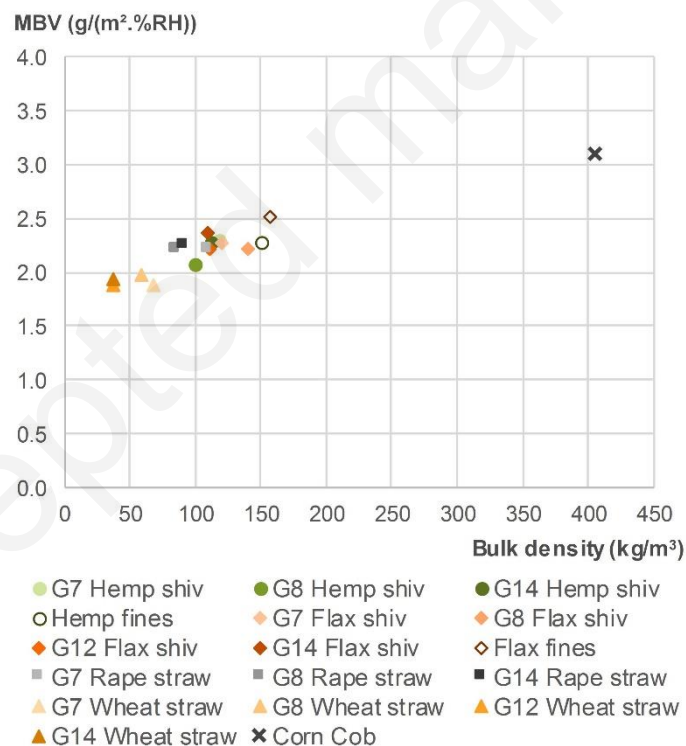*Figure 35: Moisture Buffer Value versus aggregate*

Figure 36: Moisture Buffer Value versus density

4. Synthesis

Chemical composition and physical properties of agro-resources are linked.

For shiv and straw, Figure 37 shows that the skeleton density increases linearly with the quantity of polysaccharides. The polysaccharides include cellulose, hemicellulose and pectin. As previously explained (Figure 15), the structure of agro-

resource is made of these components. The higher the quantity of polysaccharides is, the higher the skeleton density is. Indeed, the dimensional network formed by these polysaccharides is denser when the quantity of polysaccharides increases because it gives a more compact arrangement of the chains. Figure 38 shows that the thermal conductivity decreases when the quantity of polysaccharides increases. This is unexpected as the skeleton density increases with the quantity of polysaccharides. In fact, the thermal conductivity of aggregates is induced by the material porosity. The results shown on Figure 39 underline the high correlation between the decrease of thermal conductivity and the increase of open porosity of studied materials.

Figure 40 shows that the initial rate of absorption (IRA) increases linearly with the quantity of cellulose. For shiv and straw, IRA is averaged over all grades of the same agro-resource. Cellulose provides very good stiffness and strength to plant cell walls due to its molecular arrangement in microfibrils that promotes the inter- and intra-molecular hydrogen bonds. Besides a strong affinity to itself, the cellulose has also a strong affinity toward water due to its composition. Indeed, the partial charges of the cellulose and water mutually attract. So, many intermolecular hydrogen bonds are broken in the cellulose to allow new connections between cellulose chains and water molecules, leading to water bond. Water absorption causes swelling of agro-resources, hence their volume increases (Figure 41) (Chami Khazraji and Robert, 2013; Van Der Reyden, 1992).

Figure 42 gives moisture buffer value versus thermal conductivity in order to find out the best valuation on hygrothermal point of view. Each agro-resource has very close thermal conductivity and hygric capacity for different grades. Moreover, when the thermal conductivity decreases, the moisture buffer value decreases and vice-versa. Thus, (i) wheat straw appears as the best thermal insulator, with good moisture buffering ability, (ii) corn cob is the best hygric regulator but is a poor thermal insulator, (iii) hemp, flax and rape are both good thermal insulators and excellent hygric regulators (but not the best as well from both a thermal and a hygric point of view).
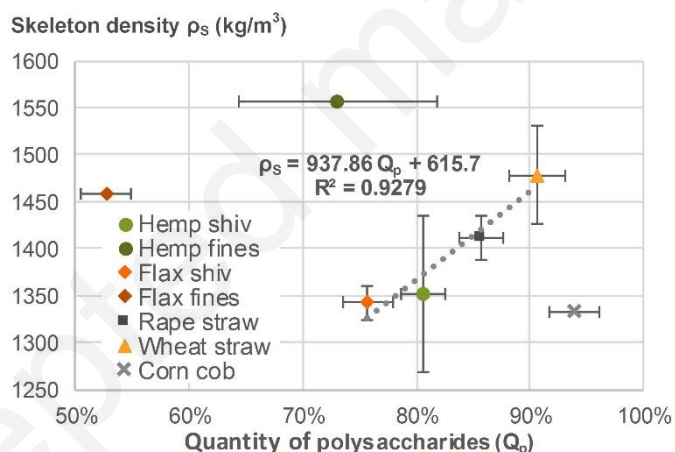

Figure 37: Skeleton density versus quantity of polysaccharides (cellulose, hemicellulose and pectin) of agro-resources
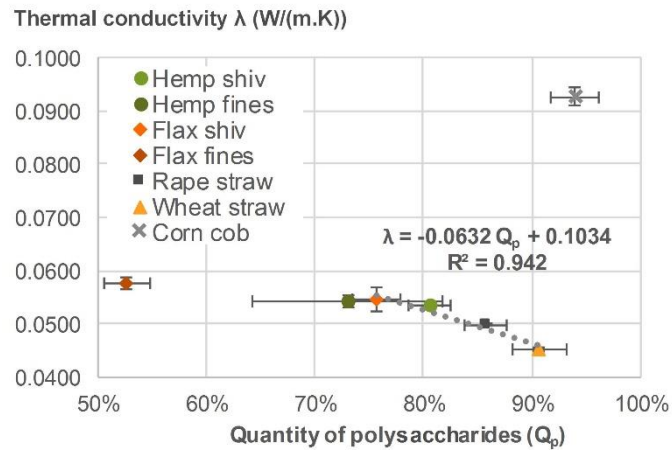
Figure 38: Thermal conductivity versus quantity of polysaccharides (cellulose, hemicellulose and pectin)
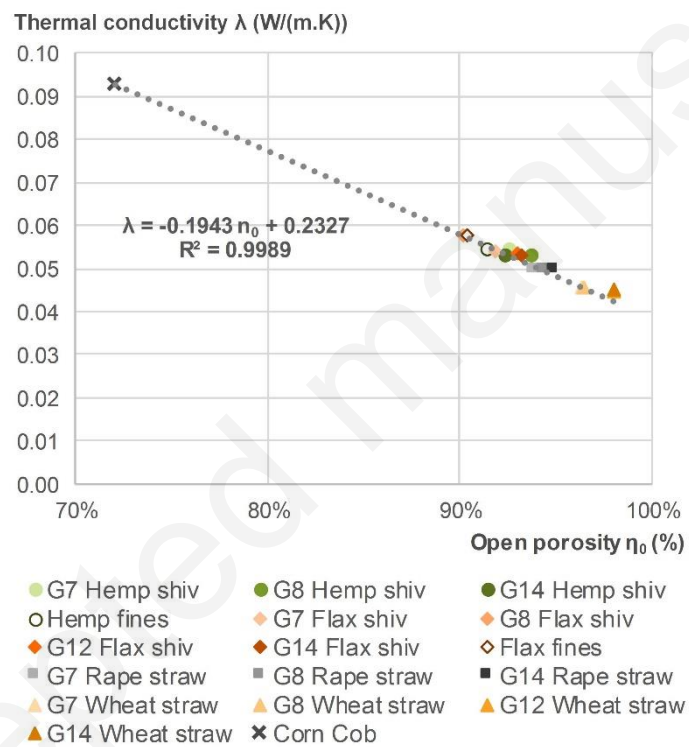

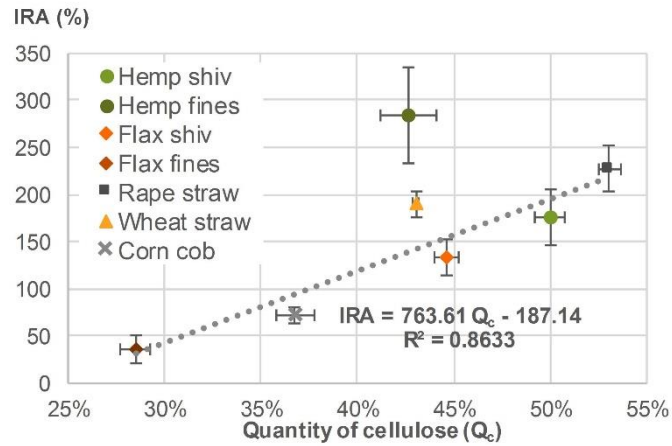*Figure 39: Thermal conductivity versus open porosity*

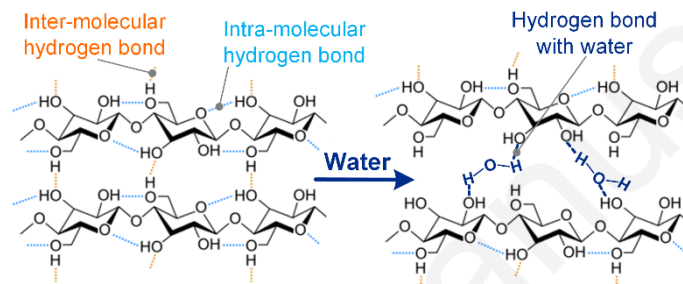*Figure 40: IRA versus quantity of cellulose of agro-resources*

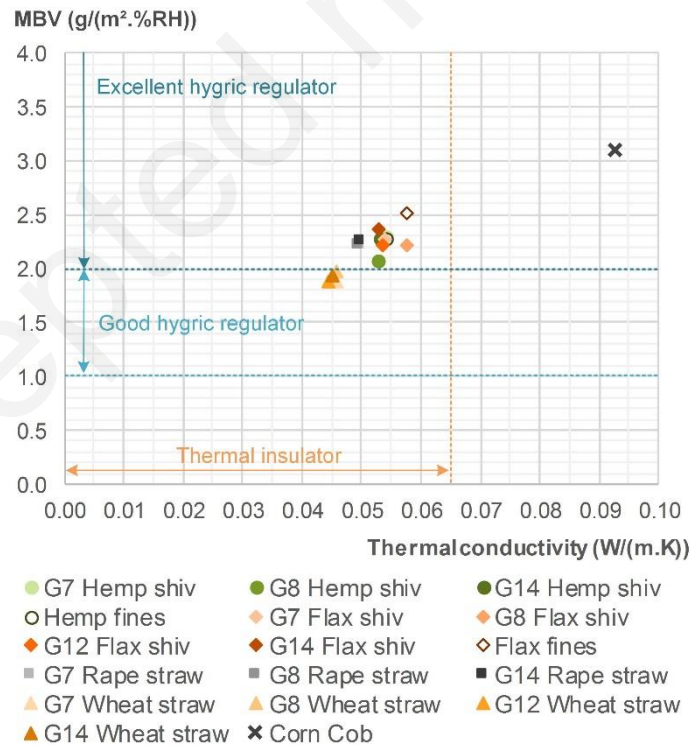*Figure 41: Hydrogen bonds in the cellulose with or without the presence of water*

Figure 42: Moisture Buffer Value versus thermal conductivity

5. Conclusions

The building industry is one of those fields in which the agro-resources' by-product can have an important role as a bio-based construction material. Substantial economic and environmental benefits can result from the adoption of this solution. This study considers five agro-resources (hemp, flax, rape, wheat and shiv) which are processed with several gradings.

The chemical investigation shows that there are large differences in the chemical composition between these lignocellulosic materials. The high cellulose, hemicellulose and lignin content should allow using such resources as gluing materials or raw materials to produce green binders.

The physical characterization shows that all aggregates are light with high porosity. On a general way, this gives them high water absorption capacity, low thermal conductivity and high moisture buffer value.

Hemp shiv, flax shiv, rape straw and wheat straw have a low thermal conductivity (lower or equal to 0.058 W/(m.K)) and are all excellent hygric regulators (MBV higher than or equal to 1.88 g/(m².%RH)). However, when the thermal conductivity decreases, the moisture buffer value decreases and vice-versa. Such bio-based aggregates can thus be used to produce thermal insulating products or indoor facing panels (like partition walls or ceiling), coupling them with mineral or green binders. In the case of use with hydraulic binder, their water absorption capacity should be taken into account to adjust water content in the mix.

Hemp fines and flax fines also show high hygrothermal performances. Regarding their particle sizes, these materials should be used as a load to produce plaster.

Finally, corn cob shows the highest performances from moisture buffering point of view. This aggregate would be very interesting if used to produce indoor facing panels (the best MBV) and may be sound-insulating material (thanks to its specific geometric shape and its high density). Such quality need to be investigated further. An interesting used could be made of corn cob as outdoor coating due its water repellency.

Both chemical and multi-physical interests of agro-resources have been underlined. Henceforth, research can go on to develop new bio-based sustainable building materials (insulating panels, plaster, bio-based concrete…).

References

Abidi, N., Cabrales, L., Haigler, C.H., 2014. Changes in the cell wall and cellulose content of developing cotton fibers investigated by FTIR spectroscopy. Carbohydr. Polym. 100, 9–16. https://doi.org/10.1016/j.carbpol.2013.01.074

AFNOR, 1997. NF V 18-122 - Aliments des animaux - Détermination séquentielle des constituants pariétaux - Méthode par traitement aux détergents neutre et acide et à l'acide sulfurique.

AFNOR, 1983. NF P75-101 - Isolants thermiques destinés au bâtiment - Définition.

Agricultural production - crops, 2016. . Eurostat Stat. Explain.

Amziane, S., Collet, F. (Eds.), 2017. Bio-aggregates Based Building Materials, RILEM State-of-the-Art Reports. Springer Netherlands, Dordrecht.

Amziane, S., Collet, F., Lawrence, M., Magniont, C., Picandet, V., Sonebi, M., 2017a. Recommendation of the RILEM TC 236-BBM: characterisation testing of hemp shiv to determine the initial water content, water absorption, dry density, particle size distribution and thermal conductivity. Mater. Struct. 50. https://doi.org/10.1617/s11527-017-1029-3

Amziane, S., Collet, F., Lawrence, M., Picandet, V., Lanos, C., Marceau, S., Pavia, S., 2017b. Bio-aggregates Based Building Materials, Springer Netherlands. ed, RILEM State-of-the-Art Reports. Amziane Sofiane and Collet Florence.

Anwar, Z., Gulfraz, M., Irshad, M., 2014. Agro-industrial lignocellulosic biomass a key to unlock the future bio-energy: A brief review. J. Radiat. Res. Appl. Sci. 7, 163–173. https://doi.org/10.1016/j.jrras.2014.02.003

Arnaud, L., Gourlay, E., 2012. Experimental study of parameters influencing mechanical properties of hemp concretes. Constr. Build. Mater. 28, 50–56. https://doi.org/10.1016/j.conbuildmat.2011.07.052

ASTM International, 1997. ASTM D854-92e, Standard Test Methods for Specific Gravity of Soil Solids by Water Pycnometer.

Balčiūnas, G., Žvironaitė, J., Vėjelis, S., Jagniatinskis, A., Gaidučis, S., 2016. Ecological, thermal and acoustical insulating composite from hemp shives and sapropel binder. Ind. Crops Prod. 91, 286–294. https://doi.org/10.1016/j.indcrop.2016.06.034

Bloomberg New Energy Finance, 2010. Next-generation ethanol and biochemicals: what's in it for Europe?

Bouasker, M., Belayachi, N., Hoxha, D., Al-Mukhtar, M., 2014. Physical Characterization of Natural Straw Fibers as Aggregates for Construction Materials Applications. Materials 7, 3034–3048. https://doi.org/10.3390/ma7043034

Bouloc, P., 2006. Le chanvre industriel: production et utilisations. France Agricole Editions.

Cappelletto, P., Brizzi, M., Mongardini, F., Barberi, B., Sannibale, M., Nenci, G., Poli, M., Corsi, G., Grassi, G., Pasini, P., 2001. Italy-grown hemp: yield, composition and cannabinoid content. Ind. Crops Prod. 13, 101–113.

Carrier, M., Loppinet-Serani, A., Denux, D., Lasnier, J.-M., Ham-Pichavant, F., Cansell, F., Aymonier, C., 2011. Thermogravimetric analysis as a new method to determine the lignocellulosic composition of biomass. Biomass Bioenergy 35, 298–307. https://doi.org/10.1016/j.biombioe.2010.08.067

Cerezo, V., 2005. Propriété mécanique thermiques et acoustiques d'un matériau à base de particules végétales : Approche expérimentale et modélisation théorique. . Ecole Nationale des Travaux Publics de l'Etat, Institut National des Sciences Appliquées de Lyon.

Chabannes, M., Bénézet, J.-C., Clerc, L., Garcia-Diaz, E., 2014. Use of raw rice husk as natural aggregate in a lightweight insulating concrete: An innovative application. Constr. Build. Mater. 70, 428–438.

Chabriac, P.A., Gourdon, E., Gle, P., Fabbri, A., Lenormand, H., 2016. Agricultural by-products for building insulation: Acoustical characterization and modeling to predict micro-structural parameters. Constr. Build. Mater. 112, 158–167. https://doi.org/10.1016/j.conbuildmat.2016.02.162

Chami Khazraji, A., Robert, S., 2013. Self-Assembly and Intermolecular Forces When Cellulose and Water Interact Using Molecular Modeling. J. Nanomater. 2013, 1–12. https://doi.org/10.1155/2013/745979

Chen, H., 2014. Chemical composition and structure of natural lignocellulose, in: Biotechnology of Lignocellulose. Springer, pp. 25–71.

Contreras, L., Gutièrrez Chavez, D., Valdivia Macedo, I., Govea Casares, R., Ramirez Carrillo, J.T., 1999. Two techniques for measuring neutral detergent (NDF) and acid detergent fibers (ADF) in forages and by-products.pdf. Arch. Zootec. 48, 351–354.

Cortella, A.R., Pochettino, M.L., 1994. Starch Grain Analysis as a Microscopic Diagnostic Feature in the Identification of Plant Material. Econ. Bot. 48, 171–181.

Diquélou, Y., Gourlay, E., Arnaud, L., Kurek, B., 2015. Impact of hemp shiv on cement setting and hardening: Influence of the extracted components from the aggregates and study of the interfaces with the inorganic matrix. Cem. Concr. Compos. 55, 112–121. https://doi.org/10.1016/j.cemconcomp.2014.09.004

Dubois, M., Gilles, K.A., Hamilton, J.K., Rebers, P.A.T., Smith, F., 1956. Colorimetric method for determination of sugars and related substances. Anal. Chem. 28, 350–356.

Dyer, T.J., 1999. Elucidating the formation and chemistry of chromophores during kraft pulping. University of Wisconsin-Stevens Point, Atlanta, Georgia.

Evon, P., 2008. Nouveau procédé de bioraffinage du tournesol plante entière par fractionnement thermo-mécano-chimique en extrudeur bi-vis: étude de l'extraction aqueuse des lipides et de la mise en forme du raffinat en agromatériaux par thermomoulage. Toulouse, France.

Fava, F., Totaro, G., Diels, L., Reis, M., Duarte, J., Carioca, O.B., Poggi-Varaldo, H.M., Ferreira, B.S., 2015. Biowaste biorefinery in Europe: opportunities and research & development needs. New Biotechnol. 32, 100–108. https://doi.org/10.1016/j.nbt.2013.11.003

Fry, S.C., 2001. Plant cell walls. eLS.

Gao, X., Kumar, R., Wyman, C.E., 2014. Fast hemicellulose quantification via a simple one-step acid hydrolysis. Biotechnol. Bioeng. 111, 1088–1096. https://doi.org/10.1002/bit.25174

Ghaffar, S.H., 2017. Straw fibre-based construction materials, in: Advanced High Strength Natural Fibre Composites in Construction. Elsevier, pp. 257–283.

Godin, B., Ghysel, F., Agneessens, R., Schmit, T., Gofflot, S., Lamaudière, S., Sinnaeve, G., Goffart, J.-P., Gerin, P.A., Stilmant, D., Delcarte, J., 2010. Détermination de la cellulose, des hémicelluloses, de la lignine et des cendres dans diverses cultures lignocellulosiques dédiées à la production de bioéthanol de deuxième génération. Biotechnol Agron Soc Env. 14, 549–560.

Graaff, J.L., van Staden, J., 1983. Seed Coat Structure of Sesbania Species. Z. Für Pflanzenphysiol. 111, 293–299. https://doi.org/10.1016/S0044-328X(83)80089-0

Greenhalf, C.E., Nowakowski, D.J., Bridgwater, A.V., Titiloye, J., Yates, N., Riche, A., Shield, I., 2012. Thermochemical characterisation of straws and high yielding perennial grasses. Ind. Crops Prod. 36, 449–459. https://doi.org/10.1016/j.indcrop.2011.10.025

Hameed, M.R., 2014. Contribution of metallic fibers on the performance of reinforced concrete. Toulouse, France.

Harris, P.J., 2006. Primary and secondary plant cell walls: a comparative overview. N. Z. J. For. Sci. 36, 36.

Herman, E.M., Larkins, B.A., 1999. Protein storage bodies and vacuoles. Plant Cell 11, 601–613.

Igathinathane, C., Pordesimo, L.O., Columbus, E.P., Batchelor, W.D., Sokhansanj, S., 2009. Sieveless particle size distribution analysis of particulate materials through computer vision. Comput. Electron. Agric. 66, 147–158. https://doi.org/10.1016/j.compag.2009.01.005

ISOBIO - Naturally High Performance Insulation, 2015.

Jeong, T.S., Oh, K.K., 2011. Optimization of fermentable sugar production from rape straw through hydrothermal acid pretreatment. Bioresour. Technol. 102, 9261–9266. https://doi.org/10.1016/j.biortech.2011.06.092

Johnson, B., Kerr, D., 2015. Flax Straw and Fibre, in: Growing Flax. Flax Council of Canada.

Kretschmer, B., Allen, B., Hart, K., 2012. Mobilising Cereal Straw in the EU to feed Advanced biofuel production. Inst. Eur. Environ. Policy.

Kymäläinen, H.-R., Sjöberg, A.-M., 2008. Flax and hemp fibres as raw materials for thermal insulations. Build. Environ. 43, 1261–1269. https://doi.org/10.1016/j.buildenv.2007.03.006

Magniont, C., Escadeillas, G., Coutand, M., Oms-Multon, C., 2012. Use of plant aggregates in building ecomaterials. Eur. J. Environ. Civ. Eng. 16, s17–s33. https://doi.org/10.1080/19648189.2012.682452

Manara, P., Zabaniotou, A., Vanderghem, C., Richel, A., 2014. Lignin extraction from Mediterranean agro-wastes: Impact of pretreatment conditions on lignin chemical structure and thermal degradation behavior. Catal. Today 223, 25–34. https://doi.org/10.1016/j.cattod.2013.10.065

Nguyen, T.T., 2010. Contribution à l'étude de la formulation et du procédé de fabrication d'éléments de construction en béton de chanvre. Université de Bretagne Sud, Lorient.

Nguyen, T.T., Picandet, V., Amziane, S., Baley, C., 2009. Etude de la formulation des bétons de chanvre pour la confection d'éléments préfabriqués par compactage. Presented at the XXVIIe Rencontres Universitaires de Génie Civil Génie Civil et Développement Durable, Saint Malo.

Nozahic, V., Amziane, S., Torrent, G., Saïdi, K., De Baynast, H., 2012. Design of green concrete made of plant-derived aggregates and a pumice–lime binder. Cem. Concr. Compos. 34, 231–241. https://doi.org/10.1016/j.cemconcomp.2011.09.002

Pérez, S., Bertoft, E., 2010. The molecular structures of starch components and their contribution to the architecture of starch granules: A comprehensive review. Starch - Stärke 62, 389–420. https://doi.org/10.1002/star.201000013

Picandet, V., Tronet, P., Baley, C., 2012. Caractérisation granulométrique des chènevottes. XXX E Rencontres AUGC-IBPSA Chambéry Savoie.

Pinto, J., Cruz, D., Paiva, A., Pereira, S., Tavares, P., Fernandes, L., Varum, H., 2012. Characterization of corn cob as a possible raw building material. Constr. Build. Mater. 34, 28–33. https://doi.org/10.1016/j.conbuildmat.2012.02.014

Pointner, M., Kuttner, P., Obrlik, T., Jager, A., Kahr, H., 2014. Composition of corncobs as a substrate for fermentation of biofuels. Agron. Res. 12, 391–396.

Rahim, M., Douzane, O., Tran Le, A.D., Langlet, T., 2016a. Effect of moisture and temperature on thermal properties of three bio-based materials. Constr. Build. Mater. 111, 119–127. https://doi.org/10.1016/j.conbuildmat.2016.02.061

Rahim, M., Douzane, O., Tran Le, A.D., Promis, G., Langlet, T., 2016b. Characterization and comparison of hygric properties of rape straw concrete and hemp concrete. Constr. Build. Mater. 102, 679–687. https://doi.org/10.1016/j.conbuildmat.2015.11.021

Rode, C., Peuhkuri, R.H., Mortensen, L.H., Hansen, K.K., Time, B., Gustavsen, A., Ojanen, T., Ahonen, J., Svennberg, K., Arfvidsson, J., others, 2005. Moisture buffering of building materials. Technical University of Denmark, Department of Civil Engineering.

Ross, K., Mazza, G., 2010. Characteristics of Lignin from Flax Shives as Affected by Extraction Conditions. Int. J. Mol. Sci. 11, 4035–4050. https://doi.org/10.3390/ijms11104035

Sain, M., Fortier, D., 2002. Flax shives refining, chemical modification and hydrophobisation for paper production. Ind. Crops Prod. 15, 1–13.

Searle, S., Malins, C., 2013. Availability of cellulosic residues and wastes in the EU. White Pap. 422.

Silva, A.S., Nunes, C., Coimbra, M.A., Guido, L.F., 2014. Composition of pectic polysaccharides in a Portuguese apple (Malus domestica Borkh. cv Bravo de Esmolfe). Sci. Agric. 71, 331–336. https://doi.org/10.1590/0103-9016-2013-0333

Sorieul, M., Dickson, A., Hill, S., Pearson, H., 2016. Plant Fibre: Molecular Structure and Biomechanical Properties, of a Complex Living Material, Influencing Its Deconstruction towards a Biobased Composite. Materials 9, 618. https://doi.org/10.3390/ma9080618

Sun, R.C., Tomkinson, J., 2000. Essential guides for isolation/purification of polysaccharides. Academic Press: Lond.

Taiz, L., Zeiger, E., 2002. Plant physiology, 3rd edn. Sinauer Associates.

Terpáková, E., Kidalová, L., Eštoková, A., Čigášová, J., Števulová, N., 2012. Chemical Modification of Hemp Shives and their Characterization. Procedia Eng. 42, 931–941. https://doi.org/10.1016/j.proeng.2012.07.486

Van Der Reyden, D., 1992. Recent Scientific Research in Paper Conservation. J. Am. Inst. Conserv. 31, 117–138. https://doi.org/10.2307/3179619

Van Soest, P.J., Robertson, J.B., Lewis, B.A., 1991. Symposium: carbohydrate methodology, metabolism, and nutritional implications in dairy cattle. J Dairy Sci 74, 3583–3597.

Vignon, M.R., Garcia-Jaldon, C., Dupeyre, D., 1995. Steam explosion of woody hemp chenevotte. Int. J. Biol. Macromol. 17, 395–404.

Voragen, A.G.J., Coenen, G.-J., Verhoef, R.P., Schols, H.A., 2009. Pectin, a versatile polysaccharide present in plant cell walls. Struct. Chem. 20, 263–275. https://doi.org/10.1007/s11224-009-9442-z

Xu, F., Sun, J.-X., Sun, R., Fowler, P., Baird, M.S., 2006. Comparative study of organosolv lignins from wheat straw. Ind. Crops Prod. 23, 180–193. https://doi.org/10.1016/j.indcrop.2005.05.008

Xu, F., Yu, J., Tesso, T., Dowell, F., Wang, D., 2013. Qualitative and quantitative analysis of lignocellulosic biomass using infrared techniques: A mini-review. Appl. Energy 104, 801–809. https://doi.org/10.1016/j.apenergy.2012.12.019

Zhang, P., Dong, S.-J., Ma, H.-H., Zhang, B.-X., Wang, Y.-F., Hu, X.-M., 2015. Fractionation of corn stover into cellulose, hemicellulose and lignin using a series of ionic liquids. Ind. Crops Prod. 76, 688–696. https://doi.org/10.1016/j.indcrop.2015.07.037